Restricted internal diffusion weakens transpiration–photosynthesis coupling during heatwaves: Evidence from leaf carbonyl sulfide exchange

Wu Sun[1], Kadmiel Maseyk[2], Céline Lett[3], Ulli Seibt[4]

[1]Department of Global Ecology, Carnegie Institution for Science, Stanford, CA 94305, USA
[2]School of Environment, Earth and Ecosystem Sciences, The Open University, Milton Keynes MK7 6AA, UK
[3]Department of Environmental Research and Innovation, Luxembourg Institute of Science and Technology, 41 Rue du Brill, L-4422 Belvaux, Luxembourg
[4]Department of Atmospheric and Oceanic Sciences, University of California, Los Angeles, CA 90095, USA

Correspondence to: Wu Sun (wsun@carnegiescience.edu)

Running head: Internal diffusion limitation revealed by COS fluxes

ORCID

- Wu Sun: 0000-0002-2333-6282
- Kadmiel Maseyk: 0000-0003-3299-4380
- Ulli Seibt: 0000-0001-6043-6269

Abstract

Increasingly frequent and intense heatwaves threaten ecosystem health in a warming climate. However, plant responses to heatwaves are poorly understood. A key uncertainty concerns the intensification of transpiration when heatwaves suppress photosynthesis, known as transpiration–photosynthesis decoupling. Field observations of such decoupling are scarce, and the underlying physiological mechanisms remain elusive. Here, we use carbonyl sulfide (COS) as a leaf gas exchange tracer to examine potential mechanisms leading to transpiration–photosynthesis decoupling on a coast live oak in a southern California woodland in spring 2013. We found that heatwaves suppressed both photosynthesis and leaf COS uptake but increased transpiration or sustained it at non-heatwave levels throughout the day. Despite statistically significant decoupling between transpiration and photosynthesis, stomatal sensitivity to environmental factors did not change during heatwaves. Instead, midday photosynthesis during heatwaves was restricted by internal diffusion, as indicated by the lower internal conductance to COS. Thus, increased evaporative demand and nonstomatal limitation to photosynthesis act jointly to decouple transpiration from photosynthesis without altering stomatal sensitivity. Decoupling offered limited potential cooling benefits, questioning its effectiveness for leaf thermoregulation in xeric ecosystems. We suggest that adding COS to leaf and ecosystem flux measurements helps elucidate diverse physiological mechanisms underlying transpiration–photosynthesis decoupling.

Keywords: carbonyl sulfide (COS or OCS), heatwaves, Mediterranean ecosystems, stomatal responses, transpiration–photosynthesis coupling, nonstomatal limitation, COS:CO_2 leaf relative uptake (LRU), coast live oak (*Quercus agrifolia*)

Summary statement

During heatwaves, plants lose more water to sustain the same level of photosynthesis, but it is unclear why they risk doing so. Here, we leverage leaf carbonyl sulfide flux measurements to show that restricted gas diffusion within leaves led to this heatwave response in a southern California oak.

1. Introduction

With climate change comes more frequent and intense heatwaves (Coumou & Robinson, 2013; F. Sun et al., 2015). Heatwaves threaten plant growth, reproduction, and survival (Breshears et al., 2021) and can trigger widespread forest die-off when coupled with droughts (Allen et al., 2010, 2015). Heatwave impacts may cascade through the food chain (Sentis et al., 2013), causing far-reaching perturbations to ecosystem resilience and the terrestrial carbon and water cycles. How well plant individuals and communities may weather heatwaves critically depends on the responses of key physiological functions, as heatwaves inhibit photosynthesis through downregulation of Photosystem II electron transport (Berry & Björkman, 1980; Sharkey, 2005; Aparecido et al., 2020; Scafaro et al., 2023) and deactivation of RuBisCO (Salvucci & Crafts-Bradner, 2004; Sharkey, 2005; Busch & Sage, 2017; Scafaro et al., 2023) and increase carbon loss via photorespiration (Ku & Edwards, 1977a, 1977b; Jordan & Ögren, 1984; Long, 1991; Dusenge et al., 2019), mitochondrial respiration (Berry & Björkman, 1980; Heskel et al., 2016; Scafaro et al., 2021), and isoprene emissions (Sharkey, 2005). Prolonged heatwaves combined with atmospheric and soil water stress amplify the risk of carbon starvation (Adams et al., 2009) or hydraulic failure (Schönbeck et al., 2022). While these physiological responses to heatwaves are well documented from controlled laboratory and field experiments, in situ field observations remain few and far between (but see, for example, Tatarinov et al., 2016; De Kauwe et al., 2019; Muller et al., 2021). Understanding plant responses to heatwaves, especially in their natural habitats with realistic climate variability, is crucial to predicting mortality, assessing ecosystem resilience, and guiding management and conservation efforts in a warming world.

A conundrum in plant responses to heatwaves concerns the decoupling of transpiration and photosynthesis (De Kauwe et al., 2019). Normally, transpiration and photosynthesis are coupled by common stomatal regulation, as stomatal opening responds to atmospheric humidity and photosynthetic assimilation rate (Cowan, 1977; Farquhar & Sharkey, 1982; Ball, 1988; Leuning, 1995; Medlyn et al., 2011) in order to optimize carbon gain against water loss (Cowan, 1977; Buckley et al., 2017; Sperry et al., 2017). However, recent evidence from leaf-scale (Urban et al., 2017), whole-canopy (Drake et al., 2018), and ecosystem-scale studies (Tatarinov et al., 2016; De Kauwe et al., 2019; Krich et al., 2022) indicates that during heatwaves, plants may keep up high transpiration despite suppressed photosynthesis, deviating from an optimal water-use strategy predicated upon marginal carbon gain (Blonder et al., 2023).

Current evidence suggests that transpiration–photosynthesis decoupling acts to protect leaves from heat damage through evaporative cooling (Urban et al., 2017; Guha et al., 2018; Drake et al., 2018; Aspinwall et al., 2019; Krich et al., 2022), provided that plants can tap into plant water

storage, soil moisture, or groundwater and have sufficient hydraulic conductivity to sustain transpiration without incurring embolism. Leaf-scale measurements on a poplar (*Populus deltoides* × *nigra*) and a loblolly pine (*Pinus taeda*) show that a high leaf temperature prompts stomata to open even more despite a decrease in leaf water potential and an increase in the intercellular CO_2 concentration (Urban et al., 2017). In water-stressed conditions, evaporative cooling caused by stomatal opening remains substantial (1°C), though much weaker than in well-watered conditions (up to 9°C; Urban et al., 2017). In an extreme heatwave experiment (> 43°C), *Eucalyptus parramattensis* trees enclosed in whole-tree chambers increased thermal tolerance of their leaves (up to 51°C) and maintained a high transpiration rate to cool leaf temperature below the temperature expected from a coupled transpiration–photosynthesis model (Drake et al., 2018). To transpire under prolonged dry conditions, plants need access to water beneath the topsoil. Deep-rooted trees may tap into root-zone soil moisture and groundwater to sustain high transpiration during heatwaves (Drake et al., 2018), as indicated by unchanged or increased sap flow in some cases (Tatarinov et al., 2016). At the regional scale, terrestrial biosphere model simulations show that continued access to groundwater increases transpiration to cool the canopy and land surface, creating a negative feedback to dampen heatwave intensity (Mu et al., 2021).

While transpiration–photosynthesis decoupling helps plants cope with heatwaves, whether the decoupling results from changes in stomatal behavior or alternative limitations (e.g., biochemical limitation to photosynthesis) remains unclear. The regulation of stomatal opening through plant hydraulics, intercellular CO_2 concentrations, and/or plant hormones such as abscisic acid (Buckley, 2017) does not seem to involve an active temperature sensing mechanism, although stomatal closure may ensue from heatwave inhibition of photosynthesis (Slot & Winter, 2017; Scafaro et al., 2023). Moreover, little is known about the prevalence of heatwave-induced decoupling of transpiration and photosynthesis across ecosystems, because field observations of carbon and water fluxes are highly underrepresented in semi-arid and arid ecosystems (van der Horst et al., 2019) where intense and prolonged heatwaves more often occur. Furthermore, ecosystem-scale flux observations often include respiration and soil evaporation components, which hinders the identification of transpiration–photosynthesis decoupling (De Kauwe et al., 2019). Semi-arid forests have also been shown to cool effectively through sensible heat fluxes (Rotenberg & Yakir, 2010, 2011; Banerjee et al., 2017, 2018; Kröniger et al., 2018; Muller et al., 2021), calling into question whether transpiration–photosynthesis decoupling is a widespread strategy for heat mitigation.

Carbonyl sulfide (COS), a trace gas in the atmosphere, can help to track photosynthesis and transpiration across scales (Montzka et al., 2007; Berry et al., 2013; Whelan et al., 2018). In

vascular plant leaves, COS is hydrolyzed via carbonic anhydrases after passing through stomata and the mesophyll (Stimler et al., 2010, 2011). This hydrolysis is a one-way reaction (Elliott et al., 1989; Protoschill-Krebs et al., 1996; Schenk et al., 2004), unlike the reversible CO_2 hydration via carbonic anhydrases (Khalifah, 1971). The general absence of a leaf COS source and the co-diffusion of COS and CO_2 across stomata allow COS uptake to be used as a proxy for photosynthetic CO_2 uptake (Stimler et al., 2010). Stomatal control of leaf COS uptake also gives rise to a mechanistic link between COS uptake and transpiration (Seibt et al., 2010; Wohlfahrt et al., 2012; Berkelhammer et al., 2014; Wehr et al., 2017; Stoy et al., 2019). At the ecosystem scale, COS flux measurements can aid in the partition of evapotranspiration into transpiration and evaporation components (Wehr et al., 2017; Berkelhammer et al., 2020). Thus, by providing an independent constraint on stomatal behavior, COS flux measurements show promise in elucidating the responses of photosynthesis (Rastogi et al., 2018a; Wohlfahrt et al., 2018; Cochavi et al., 2021) and transpiration to heatwaves.

Because the mesophyll acts as a barrier to CO_2 diffusion beyond stomata, potential heatwave impacts on mesophyll diffusion may affect photosynthesis as well as transpiration–photosynthesis decoupling (Flexas et al., 2016; Evans et al., 2021), and COS flux measurements may offer additional information on these impacts. Whereas most species surveyed so far show increased mesophyll conductance with temperature when other conditions are held unchanged (Bernacchi et al., 2002; von Caemmerer & Evans, 2015; Evans, 2021), heatwaves coupled with water stress may lead to mesophyll desiccation that restricts liquid-phase diffusion (Miyazawa et al., 2008; Tholen et al., 2008; Evans et al., 2009; Momayyezi et al., 2020). Leveraging water and COS flux measurements allows us to estimate the internal conductance to COS (Stimler et al., 2010; Sun et al., 2018), which combines mesophyll conductance and carbonic anhydrase activity (Stimler et al., 2010; Berry et al., 2013). As leaf COS uptake is typically limited by diffusion, it is commonly assumed that apparent carbonic anhydrase activity, expressed as the "biochemical conductance" (Stimler et al., 2010), is not as variable as mesophyll conductance (Wehr et al., 2017). Thus, although the internal conductance to COS cannot be equated to the mesophyll conductance to CO_2, it may serve as an integral proxy to assess the variability and relative importance of internal diffusion limitation for COS and CO_2 during heatwaves.

This study seeks to understand how leaf photosynthesis, transpiration, and COS fluxes respond to heatwaves and fluctuating atmospheric water stress, which are characteristic of Mediterranean ecosystems. Aided by the unique constraint on leaf gas exchange provided by COS flux measurements, we aim to shed light on the following questions: (i) How do stomatal and nonstomatal limitations to photosynthesis change in response to heatwaves? (ii) Do heatwaves weaken the coupling between transpiration and photosynthesis, and if so, does it result from

altered stomatal responses? We report 40-day consecutive, in situ chamber measurements of leaf COS, CO_2, and water fluxes during the transition from the end of the rainy season to the onset of summer drought in a Californian oak woodland. We characterize the diurnal variability of leaf COS and CO_2 fluxes during heatwaves and intermediate periods and examine evidence for changes in the coupling between photosynthesis and transpiration. We further show that in this Mediterranean ecosystem, it was the restricted internal diffusion rather than a change in stomatal responses that led to the observed decoupling between transpiration and photosynthesis during heatwaves. Finally, we suggest ways in which COS measurements may be used to probe into leaf physiological mechanisms underlying heatwave responses and discuss the robustness of using COS as a photosynthetic tracer in Mediterranean ecosystems.

2. Materials and methods

2.1. Site description

Leaf fluxes of COS, CO_2, and water were measured on a coast live oak (*Quercus agrifolia*) at the Stunt Ranch Natural Reserve located on the north central slope of the Santa Monica Mountains, California, USA (34.093894°N, 118.657231°W, 397 m above sea level). Stunt Ranch is part of the University of California Natural Reserve System, managed by UCLA for research and education. The site features diverse Mediterranean ecosystems composed of coastal sage scrub, chaparral, oak woodland, and riparian grassland communities, and is populated by California's native woody plant species including coast live oak (*Quercus agrifolia*), laurel sumac (*Malosma laurina*), and toyon (*Heteromeles arbutifolia*). Soils at the site are podzols (Sun et al., 2016). Average temperatures of January and July are 14°C and 24°C, respectively, and the mean annual rainfall is 541 mm, according to the 1981–2010 climatology (Daly et al., 2008; PRISM Climate Group, 2021). Annual rainfall varies wildly from year to year, as is typical for southern California. The growing season at the site aligns with the rainy season that typically spans from late fall to early spring (November to April). From 2012 to 2016 the site experienced an exceptional drought with strong rainfall deficit and record high air temperatures (Griffith and Anchukaitis, 2014).

The field campaign ran from March 29 to May 13, 2013. Rainfall was received on March 31 (2 mm) and May 5 and 6 (13.5 mm), 2013. Remotely sensed leaf area index from the MODIS sensors (MCD15A3H v006, four-day composite at 500 m resolution; Myneni et al., 2002; Myneni et al., 2015; Myneni, 2020) was 1.5 (± 0.2, 1 s.d.) $m^2\ m^{-2}$ during the study period. The mean surface pressure during the campaign was 968 hPa.

202 **2.2. Experimental setup**
203
204 We used a flow-through chamber system to measure leaf fluxes of COS, CO_2, and water (Figure
205 S1, Supporting Information). The chamber (ABT Sorime, Forges-les-Bains, France) was a
206 transparent cylinder with a height of 30 cm and a diameter of 24 cm, made of poly-(methyl 2-
207 methlypropenoate) (PMMA). We chose the PMMA material because its interaction with reduced
208 sulfur compounds is minimal. The chamber had a lid controlled by a 12 V motor switch (2947-
209 12+GS38.0500, Trident Engineering Ltd, Ascot, Berkshire, UK) to open or close (Figure S1).
210 There was an inlet and an outlet on the sides of the chamber for air to pass through. Overall, the
211 chamber design largely followed Pape et al. (2009).
212
213 We installed three chambers: one on a sunlit branch (labeled LC1), one on a shaded branch
214 (LC2), and a blank chamber for testing possible chamber artifacts in measured fluxes (LC3). The
215 blank chamber was partially shaded, and the amount of radiation it received was in between the
216 sunlit and shaded chambers. To fit an oak branch into a chamber, we kept the branch intact on
217 the tree and gently pushed it into the chamber at the bottom. The bottom of the chamber was
218 then sealed with Teflon films to form a cone-shaped wrap around the branch, fastened with cable
219 ties. See Figure S2 for a photo of the chambers in the field.
220
221 Each leaf chamber was sampled once per 90 min (March 29 to April 26, 2013) or per 60 min
222 (April 26 to May 13, 2013). During the sampling period, the chamber lid was closed for 8 min
223 to measure changes in headspace concentrations due to leaf fluxes. The chamber was otherwise
224 open to the atmosphere. Before and after the chamber measurement period, air from the open
225 chamber was sampled for 2 min each to measure background concentrations. We measured leaf
226 areas of the branches at the end of the campaign by harvesting individual leaves and scanning
227 them with an image scanner. For chamber specifications including volumes and leaf areas, see
228 Table S1.
229
230 The chambers were connected to a quantum cascade laser spectrometer (QCLS; Aerodyne
231 Research, Inc., Billerica, MA, USA) for concentration measurements. Configurations of the QCLS
232 were described in Sun et al. (2016) and are briefly recapitulated here. The QCLS measures COS,
233 CO_2, and H_2O concentrations from their respective absorption lines around 2050 cm^{-1}. A
234 recirculating chiller (Thermocube, Solid State Cooling System, Wappingers Falls, NY, USA) was
235 used to cool the laser down to its operating temperature (–26.5°C). The QCLS was set to record
236 data at 1 Hz, with the root-mean-square noise (1 σ) of COS measurement at about 3–5 pmol
237 mol^{-1}. To prevent spectral drift, a background calibration with high-purity dry N_2 gas was
238 scheduled to run every 15 min. Water vapor correction was done using the built-in method on

the instrument (D. Nelson, 2012). Although we did not implement the water vapor removal procedure described in Kooijmans et al. (2016), influences of water vapor correction parameters on COS and CO_2 fluxes were generally smaller than 1% in this dry environment (Sun et al., 2018).

We used a dry scroll pump (TriScroll 600, Agilent Technologies, Inc., Santa Clara, CA, USA) to maintain the flow of sample air into the QCLS. In addition, to avoid potential adsorption in the tubing (Synflex 0.25 inch), we used another dry scroll pump (IDP2, Agilent Technologies, Inc.) to keep the sampling lines flushed at all times. A buffer volume was placed upstream of the chambers to prevent abrupt fluctuations in concentration measurements. We monitored the flow into each chamber (Figure S3) using flow meters (AWM5104VN, Honeywell Sensing and Control, Golden Valley, MN, USA) installed at chamber inlets. The mean flow (± 1 standard deviation) was 1.87 ± 0.21 L min^{-1} into the sunlit chamber, 2.15 ± 0.26 L min^{-1} into the shaded chamber, and 1.88 ± 0.25 L min^{-1} into the blank chamber (all flow rates converted to ambient temperature and pressure).

We installed Type T (Cu–constantan) thermocouples (TC Ltd, Uxbridge, UK) inside the sunlit, shaded, and blank chambers to measure chamber air temperatures. The thermocouples were protected from solar radiation by attaching custom-made radiation shields (aluminum foils) to their tips. We were unable to measure leaf temperature because the thermocouples could not be shielded from solar radiation when attached to leaves. In addition, ambient air temperature and relative humidity were measured at approximately 1.5 m above ground in the canopy gap using a Vaisala HMP45AC probe (Vaisala, Helsinki, Finland). We also installed a photosynthetically active radiation (PAR) sensor (DPAR/CBE2BQ, Solems S.A., Palaiseau, France) alongside each chamber. Soil temperature and moisture at 5 cm depth were monitored with Stevens Hydra Probe II (Stevens Water Monitoring Systems, Inc., Portland, OR, USA) sensors, one placed 0.5 m from the tree trunk and another 4.5 m from the tree trunk in the canopy gap. We used a CR1000 data logger (Campbell Scientific, Inc., Logan, UT, USA) to record sensor data at 10 s intervals and to switch among sampling lines following a preprogrammed schedule. See Figure S4 for the meteorological conditions and Figure S5 for soil measurements during the campaign.

2.3. Flux calculation

Leaf fluxes of COS, CO_2, and H_2O were calculated based on the mass balance (Sun et al., 2018),

$$V\frac{\mathrm{d}C}{\mathrm{d}t} = q(C_\mathrm{a} - C) + FA_\mathrm{leaf}, \quad (1)$$

where V (m^3) is the chamber volume, C (mol m^{-3}) is the molar concentration of the gas (COS, CO_2, or H_2O) in the chamber headspace, C_a (mol m^{-3}) is the molar concentration of the gas in the ambient air, q (m^3 s^{-1}) is the flow rate, A_{leaf} (m^2) is the leaf area, and F (mol m^{-2} s^{-1}) is the leaf flux to be estimated (see Table S2 for a list of symbols). When the chamber is open to the atmosphere, chamber headspace concentration is the same as the ambient concentration, that is, $C|_{t=0} = C_a$. This initial condition allows us to solve the headspace concentration as a function of time,

$$C(t) = C_a + \frac{FA_{leaf}}{q}\left[1 - \exp\left(-\frac{qt}{V}\right)\right]. \quad (2)$$

Therefore, the flux is,

$$F = \frac{q(C - C_a)}{A_{leaf}\left[1 - \exp\left(-\frac{qt}{V}\right)\right]}. \quad (3)$$

However, due to the presence of random measurement uncertainty and turbulent fluctuations in ambient and chamber headspace concentrations, we leveraged all measurements in a sampling period (Figure S6) to derive a robust estimate of F. We fit the following regression,

$$y = \frac{FA_{leaf}}{q}(1 - x) + b + \epsilon, \quad (4)$$

where $y = C - C_a$, $x = \exp(-qt / V)$, b is the intercept to account for potential bias in C_a, and ϵ is the combined error term. From the regression we obtained an estimate of the flux F, as well as its standard error, from the fitted slope. See Figure S6 for a typical example of the changes in chamber headspace concentrations during a sampling period and the fitted curves.

We used automated software for flux calculation to ensure quality and reproducibility. Raw data from meteorological sensors and the QCLS were ingested by a custom-made software package, PyChamberFlux (v0.13.1.a) (Sun, 2018), to produce tabulated output of chamber fluxes, biometeorological variables, and curve-fitting diagnostics. The same software package was previously used to calculate leaf fluxes reported in Kooijmans et al. (2019). Data quality control was performed similarly to that in Sun et al. (2018).

2.4. Corrections for possible blank chamber COS effects

Throughout the campaign, the blank chamber (LC3) showed minor COS emissions that coincided with high temperatures during the day. We found that COS emissions from the blank

chamber increased with chamber air temperature but did not correlate with radiation after the temperature effect was accounted for. An empirical relationship between blank chamber COS emissions ($F_{\mathrm{COS,blank}}$, pmol m^{-2} s^{-1}) and chamber air temperature (T, °C) was fitted to correct the measurements of leaf COS fluxes in branch chambers (LC1 and LC2) for possible chamber-related emission artifacts (Figure S7, SI):

$$F_{\mathrm{COS,blank}} = \theta_0 + \exp(\theta_1 + \theta_2 T) + \epsilon \quad (5)$$

where θ_0, θ_1, and θ_2 are coefficients and ϵ indicates the residuals, assumed to follow a Gaussian distribution. See Table S3, SI for a summary table of the regression results.

The blank chamber COS effect represented by Eq. (5) was then calculated for both sunlit and shaded leaf chambers and subtracted from COS flux measurements. Overall, the chamber effect was bounded by 0.7 pmol m^{-2} s^{-1} for the sunlit chamber and 0.5 pmol m^{-2} s^{-1} for the shaded chamber (95th percentiles). Additional uncertainty introduced by the chamber COS effect was also included in the uncertainty of COS flux measurements following Gaussian error propagation (Figure S8, SI).

Because blank chamber CO_2 and H_2O fluxes were minor and not statistically different from zero (Figures S9 and S10 and Table S3, SI), no such corrections were made on branch chamber (LC1 and LC2) CO_2 and H_2O fluxes.

2.5. Calculation of derived variables

Vapor pressure deficit (VPD, Pa) was calculated from chamber air temperature (T, °C) and water vapor mixing ratio (x_{H2O}, mmol mol^{-1}) measured by the QCLS.

$$\mathrm{VPD} = e_{\mathrm{sat}}(T) - x_{\mathrm{H2O}}\, p, \quad (6)$$

where e_{sat} (Pa) is the saturation vapor pressure of water (Goff & Gratch, 1946) and p (Pa) is the ambient pressure. Similarly, relative humidity (RH, 0–1) of the chamber air was calculated by

$$\mathrm{RH} = \frac{\chi_{\mathrm{H_2O}}\, p}{e_{\mathrm{sat}}(T)}. \quad (7)$$

Stomatal conductance to water vapor ($g_{\mathrm{s,H2O}}$, mol m^{-2} s^{-1}) was calculated from water fluxes (E, mmol m^{-2} s^{-1}) and VPD:

$$g_{s,H_2O} = \frac{p}{VPD} E. \quad (8)$$

In doing so, we assumed that leaf boundary layer conductance to water vapor was negligible compared with stomatal conductance, given that the flow rate of around 2 L min^{-1} (Figure S3, SI) maintained a flow speed of around 1 m s^{-1} at the inlet and that even very weak turbulence within the chamber may sustain a boundary layer conductance that is an order of magnitude higher than that of the total conductance (Supplementary Notes S1 and Figures S11 and S12, SI). Because leaf temperatures were not available, we used VPD in the chamber air to approximate the leaf-to-air VPD. While this assumption might be influenced by differences between leaf and air temperatures, leaf energy balance simulations for midday sunlit conditions indicate that the leaf-to-air temperature differences were not substantial under even slightly turbulent conditions (Supplementary Notes S2 and Figure S13, SI).

Stomatal conductances to COS ($g_{s,COS}$, mol m^{-2} s^{-1}) and to CO_2 ($g_{s,CO2}$, mol m^{-2} s^{-1}) were calculated from the molecular diffusivity ratio between H_2O and COS ($R_{H2O-COS}$) and that between H_2O and CO_2 ($R_{H2O-CO2}$), respectively (Stimler et al., 2010; Seibt et al., 2010):

$$g_{s,COS} = \frac{g_{s,H_2O}}{R_{H_2O-COS}}, \quad (9a)$$

$$g_{s,CO_2} = \frac{g_{s,H_2O}}{R_{H_2O-CO_2}}, \quad (9b)$$

where $R_{H2O-COS} = 1.94$ and $R_{H2O-CO2} = 1.60$.

The internal conductance to COS ($g_{i,COS}$, mol m^{-2} s^{-1}), defined as the combination of mesophyll conductance to COS diffusion and biochemical activity of COS hydrolytic reactions (Stimler et al., 2010; Berry et al., 2013), is calculated by

$$g_{i,COS} = \left(-\frac{\chi_{COS}}{F_{COS}} - \frac{1}{g_{s,COS}}\right)^{-1}, \quad (10)$$

where x_{COS} (pmol mol^{-1}) is the mixing ratio of COS in the chamber and F_{COS} (pmol m^{-2} s^{-1}) is the COS flux. We restrict the calculation to conditions when there is net COS uptake ($F_{COS} < 0$) to reduce the impact of potential COS emissions.

We define the fraction of internal resistance to COS in total resistance to COS as a nondimensional index for internal diffusion limitation:

$$f_{\mathrm{IDL}} = \frac{r_{\mathrm{i,cos}}}{r_{\mathrm{s,cos}}+r_{\mathrm{i,cos}}} = \frac{\frac{1}{g_{\mathrm{i,cos}}}}{\frac{1}{g_{\mathrm{s,cos}}}+\frac{1}{g_{\mathrm{i,cos}}}} = \frac{g_{\mathrm{s,cos}}}{g_{\mathrm{s,cos}}+g_{\mathrm{i,cos}}}, \quad (11)$$

where $r_{s,COS}$ and $r_{i,COS}$ (m^2 s mol^{-1}) are stomatal and internal resistances to COS (i.e., the inverses of the corresponding conductances), respectively. Note that the internal diffusion limitation index is calculated only when there is net uptake of COS.

The COS : CO_2 leaf relative uptake (LRU) is the ratio between COS and CO_2 leaf uptake rates normalized against their respective ambient concentrations (Campbell et al., 2008; Stimler et al., 2010):

$$\mathrm{LRU} = \frac{F_{\mathrm{cos}}}{\chi_{\mathrm{cos}}}\frac{\chi_{\mathrm{co_2}}}{F_{\mathrm{co_2}}}, \quad (12)$$

where F_{CO2} (μmol m^{-2} s^{-1}) is the leaf CO_2 flux and x_{CO2} (μmol mol^{-1}) is the mixing ratio of CO_2 in the chamber.

2.6. Heatwave responses

We define heatwave days with a criterion of the daily maximum air temperature exceeding 30°C in April or 32°C in May, equivalent to the 96th percentiles of April and May daily maximum temperatures in 1981–2010 climatology (Figure S14, SI; Daly et al., 2008; PRISM Climate Group, 2021), respectively. By this definition, April 20, May 2–3, and May 11–13, 2013 were heatwave days (Figure S15, SI) and were binned together to derive the median diurnal cycles of fluxes during heatwaves. The rest of the time series were binned to derive the median diurnal cycles of COS, CO_2, and water fluxes during normal periods.

In comparing stomatal and internal conductance estimates between normal periods and heatwaves, we focused on the difference between empirical distributions of conductance estimates to alleviate the potential impact of uncertainty in these estimates. The internal conductance to COS carries a larger relative uncertainty than stomatal conductance, because the former incorporates uncertainties in both COS and H_2O fluxes (Eq. 10). However, random uncertainties are unlikely to bias median estimates. Furthermore, to reduce the impact of heatwave-driven COS emissions on the calculated internal conductance to COS, we did the calculation only when there was net COS uptake (Sect. 2.5).

2.7. Testing transpiration–photosynthesis coupling

We examined the coupling of transpiration and photosynthesis in two ways — the apparent coupling between transpiration and photosynthesis and the intrinsic coupling between stomatal conductance and photosynthesis. We consider a consistent increase in transpiration (or stomatal conductance) at the same photosynthetic rate during heatwaves to indicate relaxed coupling (Urban et al., 2017; Drake et al., 2018; De Kauwe et al., 2019; Krich et al., 2022) because this makes plants appear less capable of regulating water use to maximize carbon gain. This definition centers on the phenomenon but does not prescribe its physiological basis.

The apparent coupling is defined by the linear relationship between transpiration and photosynthesis, modified by VPD (De Kauwe et al., 2019), when assuming a constant ambient CO_2 concentration,

$$E \sim A_n \, \mathrm{VPD}^{1/2} \tag{13}$$

where E is the transpiration rate (mmol m^{-2} s^{-1}) and $A_n = -F_{CO2}$ is the net photosynthetic CO_2 assimilation rate (μmol m^{-2} s^{-1}). While this relationship is inspired by the Medlyn equation of optimal stomatal behavior (Medlyn et al., 2011), it is often applied empirically at the ecosystem scale (Zhou et al., 2014; De Kauwe et al., 2019; J. Nelson et al., 2020). The slope of this relationship is sometimes known as the "underlying" water use efficiency (Zhou et al., 2016; J. Nelson et al., 2020).

We also tested the intrinsic (stomatal) coupling between transpiration and photosynthesis using the Ball–Woodrow–Berry equation of stomatal conductance (Ball et al., 1987; Ball, 1988),

$$g_{s,H_2O} = m \frac{A_n \, \mathrm{RH}}{\chi_{CO2}} + g_0, \tag{14}$$

where m (dimensionless) is the slope that characterizes the composite stomatal sensitivity to environmental factors, and g_0 (mol m^{-2} s^{-1}) is the minimum stomatal conductance. Although the original Ball–Woodrow–Berry equation uses CO_2 mixing ratio and relative humidity *at the leaf surface*, given that the inlet flow in the sampling system (~2 L min^{-1}; Figure S3, SI) might have enhanced laminar convection in the leaf boundary layer (Supplementary Notes S1), we assumed that the differences in CO_2 and H_2O concentrations between the chamber air and the leaf surface were not substantial.

To examine the presence of heatwave-induced decoupling between transpiration and photosynthesis, as well as its potential origin in stomatal behavior, we tested the statistical significance of the differences in the regression coefficients between normal periods and heatwaves.

The apparent coupling between transpiration (E, mmol m^{-2} s^{-1}) and photosynthesis (A_n, μmol m^{-2} s^{-1}) was tested using a linear relationship following Eq. (13):

$$E = (1 + \alpha_0\delta)\beta_0 + (1 + \alpha_1\delta)\beta_1 A_n\sqrt{\mathrm{VPD}}, \quad (15)$$

where δ is a binary indicator of heatwave events (0 for normal periods and 1 for heatwaves), β_0 (mmol m^{-2} s^{-1}) and β_1 (mmol μmol^{-1} $Pa^{-1/2}$) are the intercept and slope in normal conditions, and α_0 (dimensionless) and α_1 (dimensionless) represent heatwave modification (when $\delta = 1$) to the intercept and the slope. Therefore, if $\alpha_0\beta_0$ (for the intercept) or $\alpha_1\beta_1$ (for the slope) is statistically different from zero, there is a statistically significant change to the apparent coupling between transpiration and photosynthesis during heatwaves.

Similarly, the coupling between stomatal conductance ($g_{s,H2O}$, mol m^{-2} s^{-1}) and photosynthesis (A_n, μmol m^{-2} s^{-1}) is described by a linear relationship following Eq. (14):

$$g_{s,H_2O} = (1 + \gamma_0\delta)g_0 + (1 + \gamma_1\delta)m\frac{A_n\,\mathrm{RH}}{\chi_{CO2}}, \quad (16)$$

where δ is the same binary indicator of heatwave events as in Eq. (15), and γ_0 and γ_1 (both dimensionless) represent heatwave modifications to the intercept and the slope, respectively. Again, we can tell whether there is a statistically significant change to the coupling between stomatal conductance and photosynthesis during heatwaves by examining if $\gamma_0 g_0$ (for the intercept) or $\gamma_1 m$ (for the slope) is statistically different from zero. See Table 1 for the fitted regression coefficients.

2.8. Estimation of potential cooling effects from transpiration–photosynthesis decoupling for sunlit leaves

If statistically robust decoupling between transpiration and photosynthesis is detected during heatwaves, we may follow a simple leaf energy balance model to estimate the potential cooling benefits from such decoupling for sunlit leaves. This estimation was not applied to shaded leaves due to the lack of data to fully inform canopy radiative transfer, in particular, the distribution of

diffuse shortwave radiation and longwave radiation within the canopy. At a steady state, the energy balance at the leaf surface follows (Campbell & Norman, 1998; Bonan, 2019),

$$R_{\mathrm{abs}} = 2\varepsilon_{\mathrm{leaf}}\sigma_{\mathrm{SB}}T_{\mathrm{leaf}}^4 + 2c_{p,\mathrm{m}}g_{\mathrm{b,H}}(T_{\mathrm{leaf}} - T) + \lambda E, \quad (17)$$

where R_{abs} (W m^{-2}) is the net absorbed radiation, $\varepsilon_{\mathrm{leaf}}$ (dimensionless) is the leaf emissivity in the thermal infrared band, assumed to be 0.95 (Richardson et al., 2021), $\sigma_{\mathrm{SB}} = 5.670374419 \times 10^{-8}$ W m^{-2} K^{-1} is the Stefan–Boltzmann constant (Tiesinga et al., 2021), T_{leaf} (K) is the leaf temperature, $c_{p,\mathrm{m}} = 29.08$ J mol^{-1} K^{-1} is the molar specific heat capacity of air at constant pressure, $g_{\mathrm{b,H}}$ (mol m^{-2} s^{-1}) is the leaf boundary layer conductance to heat (an unknown to be tested against), T (K) is the air temperature, and λ (J mol^{-1}) is the enthalpy of vaporization of water (Henderson-Sellers, 1984). For simplicity, we assume that R_{abs} is dominated by shortwave radiation, estimated from PAR measurements (Meek et al., 1984), and that leaf albedo in the shortwave band is 0.10 (Hollinger, 1992).

Assuming that heatwave-induced transpiration–photosynthesis decoupling leads to an increase of ΔE in transpiration relative to what would be expected if such decoupling did not happen and that this extra amount of transpiration leads to extra cooling of leaf temperature by ΔT_{leaf}, the leaf energy balance can be described as,

$$R_{\mathrm{abs}} = 2\varepsilon_{\mathrm{leaf}}\sigma_{\mathrm{SB}}(T_{\mathrm{leaf}} - \Delta T_{\mathrm{leaf}})^4 + 2c_{p,\mathrm{m}}g_{\mathrm{b,H}}(T_{\mathrm{leaf}} - T - \Delta T_{\mathrm{leaf}}) + \lambda(E + \Delta E), \quad (18)$$

Subtracting Eq. (18) from Eq. (17) yields an implicit equation linking ΔT_{leaf} to ΔE, with $g_{\mathrm{b,H}}$ being an unknown parameter due to lack of concurrent wind speed measurements,

$$2\varepsilon_{\mathrm{leaf}}\sigma_{\mathrm{SB}}\left[T_{\mathrm{leaf}}^4 - (T_{\mathrm{leaf}} - \Delta T_{\mathrm{leaf}})^4\right] + 2c_{p,\mathrm{m}}g_{\mathrm{b,H}}\Delta T_{\mathrm{leaf}} - \lambda\Delta E = 0. \quad (19)$$

Assuming possible values of $g_{\mathrm{b,H}}$ at 0.25, 0.5, 1.0, and 2.0 mol m^{-2} s^{-1} under typical wind regimes at the site (Supplementary Notes S1 and Figures S11 and S12, SI), we solved for the potential cooling benefits during heatwaves, ΔT_{leaf}, for these scenarios from Eqs. (18) and (19). Dimensional analysis of Eq. (19) suggests that the numerical solution of ΔT_{leaf} is not sensitive to the precise value of T_{leaf} when $g_{\mathrm{b,H}}$ is large.

3. Results

3.1. Diurnal cycles and environmental controls of leaf COS and CO_2 fluxes

The median diurnal cycle of leaf COS uptake mirrored that of CO_2 uptake in both the sunlit and shaded chambers (Figure 1a, b). In both chambers, leaf uptake of COS and CO_2 peaked around 10:00 local time (Pacific Daylight Time or UTC–7) rather than at solar noon (c. 13:00). Following the morning peak of uptake was a prolonged midday depression interval that lasted until mid-afternoon (15:00 or 16:00). Smaller peaks of COS and CO_2 uptake occurred in the mid-afternoon. Overall, the diurnal cycles of COS and CO_2 fluxes were closely aligned in terms of the timing of peak uptake and the duration of midday depression, reflecting a common diffusional control of these fluxes.

The suppression of uptake around midday was stronger in the sunlit chamber than in the shaded chamber (Figure 1a vs. b). Notably, at the height of midday depression (around 14:00), net COS uptake was completely suppressed in the sunlit chamber (Figure 1a), whereas in the shaded chamber it dropped by 53% (from –1.8 to –0.8 pmol m^{-2} s^{-1}) with respect to the morning peak (Figure 1b). Similarly, CO_2 uptake at the height of midday depression declined more sharply with respect to the morning peak in the sunlit chamber (–73%, from –2.0 to –0.5 μmol m^{-2} s^{-1}; Figure 1a) than in the shaded chamber (–50%, from –1.4 to –0.7 μmol m^{-2} s^{-1}; Figure 1b).

At the daily timescale, vapor pressure deficit (VPD) exerted a stronger control on the diurnal cycles of leaf COS and CO_2 fluxes than photosynthetically active radiation (PAR). Despite a stark contrast in the magnitudes of PAR (up to five times; Figure 1e vs. f), peak CO_2 uptake in the shaded chamber (–1.4 μmol m^{-2} s^{-1}) was only 29% lower than that in the sunlit chamber (–2.0 μmol m^{-2} s^{-1}). This small difference in CO_2 uptake in spite of large difference in PAR was likely because the shaded leaves had a higher maximum photosynthetic capacity and reached light saturation at lower PAR than did the sunlit leaves, as indicated by single-leaf (Supplementary Notes S3 and Figure S16, SI) and branch-level light response curves (Figure S17, SI).

The midday depression patterns (Figure 1a vs. b) differed between the sunlit and shaded chambers (acute vs. mild) because of different levels of diffusional limitation (Figure 1c vs. d) regulated by radiation (Figure 1e vs. f) and humidity (Figure 1g vs. h). In both chambers, stomatal conductance to COS peaked around 09:00 (Figure 1c, d; see also Figure S18, SI for water fluxes, stomatal conductance to water vapor, and internal-to-ambient CO_2 concentration ratios) when PAR started to climb but VPD was not yet high enough to curb stomatal opening. Stomatal conductance remained low throughout the rest of the day despite a late afternoon

decline in VPD. Due to the lower VPD (Figure 1h), leaves in the shaded chamber were able to maintain higher stomatal conductance (23% higher) than those in the sunlit chamber between 12:00 and 15:00 (t = –2.29 and $p < 0.05$ (N_1 = 113, N_2 = 114) in a two-sided t-test on two independent samples; Figure S19, SI).

A sharp increase in internal diffusion limitation accompanied the midday depression of leaf fluxes, as indicated by the internal conductance to COS (Figure 1c, d). For COS, the internal conductance exceeded stomatal conductance in the early morning but quickly dipped below the latter by midday. The internal conductance to COS was the lowest around the time when VPD peaked (compare Figure 1c with g, and Figure 1d with h). Thus, stomatal conductance and internal conductance jointly regulated the diurnal cycles of leaf COS and CO_2 fluxes.

3.2. Nighttime COS uptake

Nighttime COS uptake was minimal compared with daytime uptake (Figure 1a, b; Figure S20, SI): –0.07 ± 0.26 pmol m^{-2} s^{-1} (N = 447) in the sunlit chamber and –0.07 ± 0.30 pmol m^{-2} s^{-1} (N = 427) in the shaded chamber. This finding aligns with the negligible stomatal conductance at night (Figure S21, SI). In contrast, nighttime CO_2 emissions were small but less variable and statistically distinguishable from zero (see also Figure S22, SI): 0.14 ± 0.09 µmol m^{-2} s^{-1} (N = 447) in the sunlit chamber and 0.10 ± 0.11 µmol m^{-2} s^{-1} (N = 427) in the shaded chamber. These results indicate that the nighttime COS budget (⩽5% of total leaf COS uptake; Table S4) is not a major concern when using COS as an integrated tracer for photosynthesis in this oak woodland, unlike in forests (Commane et al, 2015; Kooijmans et al., 2017; Rastogi et al., 2018b; Spielmann et al., 2019) or in an alpine grassland (Spielmann et al., 2019). This observation also underscores the need for biome-specific parameterization of nighttime stomatal conductance in COS-enabled terrestrial biosphere models (e.g., Maignan et al., 2021; Kooijmans et al., 2021).

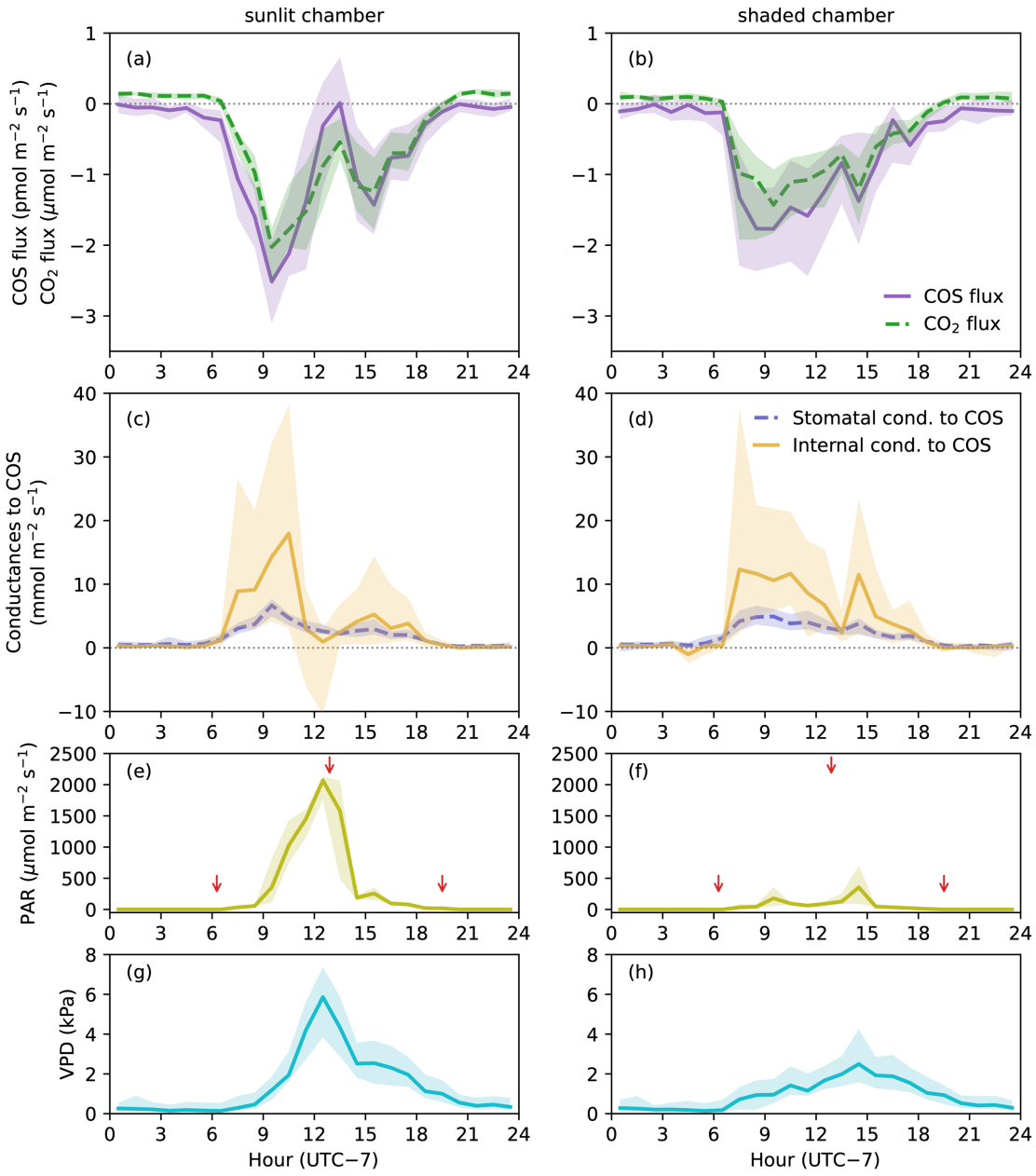

Figure 1. Median diurnal cycles of COS (solid purple lines) and CO_2 (dashed green lines) fluxes (a, b), stomatal (dashed slate blue lines) and internal (solid dark gold lines) conductances to COS (c, d), photosynthetically active radiation (e, f), and vapor pressure deficit (g, h) in the sunlit (left) and the shaded (right) chambers, binned by the hour of the day (Pacific Daylight Time or UTC–7) over the entire campaign. Note that stomatal conductance to water vapor is about twice that to COS (c, d). Shaded areas indicate the corresponding interquartile ranges (i.e., from the 25th percentile to the 75th percentile) at each hour. Dotted gray lines indicate zero fluxes (a, b) or conductances (c, d). Note that COS and CO_2 fluxes are in different units (a and b). Red arrows (e, f) mark approximate sunrise, solar noon, and sunset times during the campaign.

3.3. The temperature response of leaf COS fluxes

As temperature increased, net COS emissions from leaves increased in frequency and magnitude in the sunlit chamber but remained rare in the shaded chamber (Figure 2). Although temperature is not the only driver of leaf COS fluxes, as indicated by the scatter (Figure 2), quantile regressions allowed us to differentiate responses to temperature when the leaf is a net sink of COS (5th percentile) and when it is a net source (95th percentile). For both chambers, the 5th percentile regression lines (net COS uptake) showed a trend of increasing COS uptake with temperature, indicating primarily a day–night temperature contrast (low COS uptake at night coincides with low temperature) and the indirect influence of PAR on COS uptake through stomatal responses (temperature and PAR diurnal cycles are correlated). However, the 95th percentile regression lines (net COS emissions) showed a trend of increasing COS emissions with temperature in the sunlit chamber but not in the shaded chamber. In the sunlit chamber, there was virtually no significant COS uptake observed at above 40°C, and leaves behaved as a net COS source with a mean flux of 0.74 ± 0.86 pmol m^{-2} s^{-1} (N = 33). Leaves in the shaded chamber, by contrast, showed less frequent COS emissions due to lower temperatures. Therefore, the propensity of leaves acting as a net COS source increases with temperature, but such propensity rarely manifests itself at low and intermediate temperatures (T < 40°C; Figure S23, SI).

Surprisingly, in the low temperature range (e.g., 10–15°C), there were also isolated incidences of COS emissions, although the number of net emission observations were dwarfed by the number of net uptake observations (Figure 2). These low-temperature COS emissions could be radiation driven. However, logistic regression showed that the occurrence of COS emissions is slightly better explained by temperature than by PAR, and including both temperature and PAR as predictors does not markedly improve the classification of emission vs. uptake cases compared with using each predictor alone (Figure S23, SI). Because high radiation and high temperature conditions often co-occur in the field, the role of high radiation in leaf COS emissions cannot be ruled out.

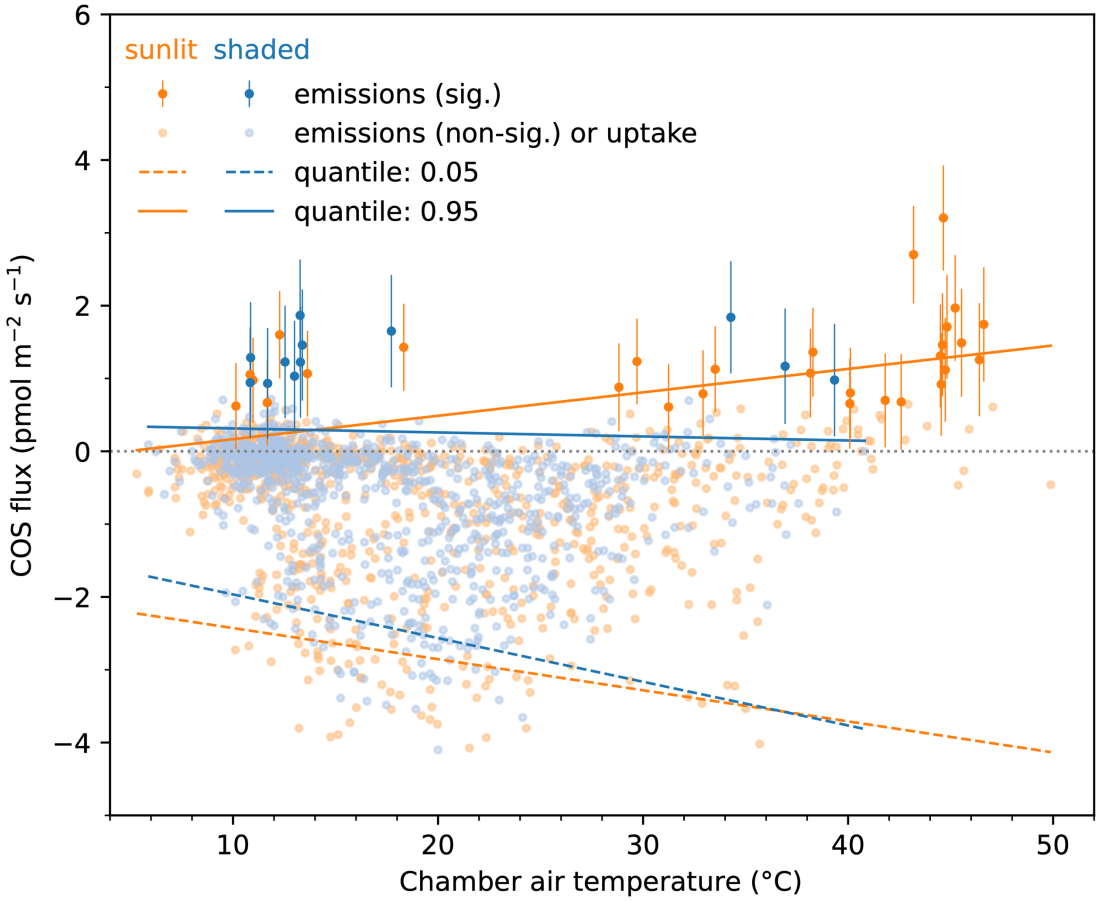

Figure 2. Heat extremes trigger COS emissions in leaves, which become dominant at temperatures above 40°C. Temperature response of leaf COS fluxes in the sunlit chamber (orange) and the shaded chamber (blue). Statistically significant COS emissions are shown in solid dots with error bars indicating the 95% confidence interval. Error bars incorporate both uncertainty from flux estimation (Sect. 2.3) and that from blank chamber effect correction (Sect. 2.4). Emissions that are not statistically significant and all net uptake fluxes are indicated by transparent dots (error bars omitted for visual clarity). Also shown are the 5th (dashed) and 95th (solid) percentile regression lines against temperature for both chambers, applied to all data for each chamber. Leaves in the sunlit chamber show a higher propensity for COS emissions at high temperatures than leaves in the shaded chamber, as indicated by the slopes of their 95% percentile regression lines (solid orange line vs. solid blue line), likely because that air temperature in the shaded chamber rarely reached 40°C for emissions to pick up.

3.4. Contrasts between leaf fluxes in normal and heatwave periods

Meteorological conditions did not vary much from day to day during the campaign period except for heatwaves and a handful of overcast days (Figure S15, SI). In normal periods, daytime temperatures peaked at 38°C at midday in the sunlit chamber (Figure S24a, SI) and 26°C in early afternoon in the shaded chamber (Figure S24b, SI). Nighttime temperature was consistently around 12°C in both chambers. During heatwaves, daytime peak temperatures shot up to 46°C in the sunlit chamber and 38°C in the shaded chamber, and nighttime temperatures were elevated to 18°C (Figure S24a and b). Heatwaves brought about an increase of VPD by 4 kPa during the daytime and 1 kPa at night in both chambers (Figure S24c and d). No substantial difference in the diurnal cycles of PAR was detected between normal periods and heatwaves (Figure S24e and f). The steady meteorological conditions during non-heatwave periods allowed us to compare representative diurnal cycles of leaf fluxes.

Heatwaves substantially suppressed daytime leaf uptake of COS and CO_2 and ramped up transpiration in both the sunlit and shaded chambers (Figure 3). Overall, heatwave impacts were stronger in the sunlit chamber than in the shaded chamber due to higher temperatures in the former (Figure S24, SI).

Both leaf COS and CO_2 fluxes showed decreased peak uptake rates and a complete suppression of the smaller afternoon peak in uptake (Figure 3a–d). The sunlit chamber showed COS emissions at midday during heatwaves (Figure 3a), as expected from the temperature response of COS fluxes (Figure 2). Conversely, in the shaded chamber, COS fluxes were near zero after the morning peak uptake during heatwaves, without noticeable COS emissions (Figure 3b). This difference was mainly because the shaded chamber had lower temperatures (rarely exceeding 40°C) than the sunlit chamber (Figure 2; see also Figure S24, SI). For leaves in the shaded chamber, heatwaves also caused the morning peak uptake of COS and CO_2 to occur one or two hours earlier and drop off more abruptly than during normal periods (Figure 3b, d). Similar to COS uptake, leaf CO_2 uptake during heatwaves also declined rapidly after mid-morning, and was close to zero throughout the afternoon (Figure 3c, d). These patterns were also largely consistent among heatwave events when they were examined individually (Figures S25 and S26, SI).

Contrary to suppressed leaf COS and CO_2 uptake, transpiration increased during heatwaves (Figure 3e, f). For the sunlit chamber, heatwaves increased the peak transpiration but did not change the shape of the diurnal cycle. For the shaded chamber, heatwaves substantially increased transpiration in the early morning and shifted the timing of peak transpiration earlier, but did not change afternoon transpiration. Overall, the higher transpiration rates during heatwaves

indicated that the increase in VPD outweighed the decrease in stomatal conductance in controlling transpiration.

Although heatwaves led to higher nighttime temperatures, no significant changes in nighttime leaf respiration (Figure 3c, d) were detected.

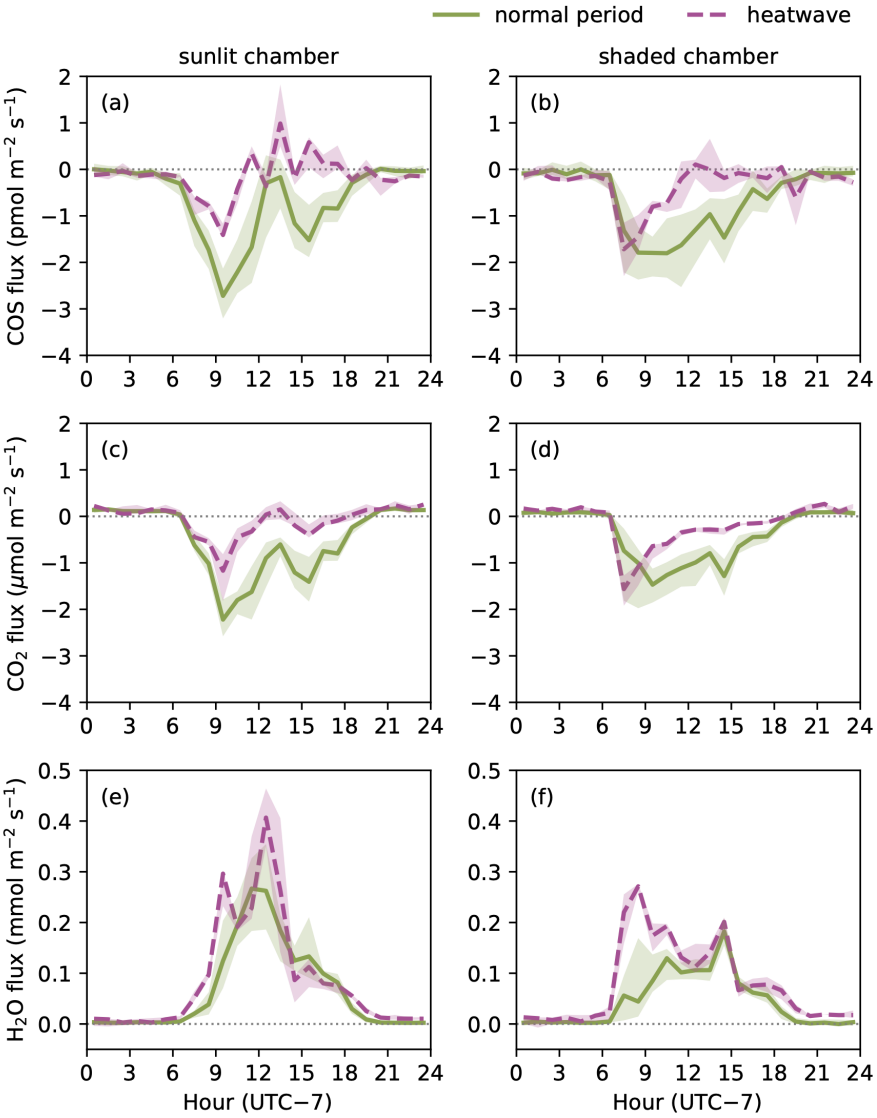

Figure 3. Contrasting diurnal cycles of leaf fluxes of COS (a and b), CO_2 (c and d), and water vapor (e and f) between normal (non-heatwave, solid olive lines) periods and heatwaves (dashed violet lines). Left column (a, c, e), diurnal cycles of leaf fluxes in the sunlit chamber; right column (b, d, f), diurnal cycles of leaf fluxes in the shaded chamber. Lines indicate median diurnal cycles binned by the hour, and shaded areas indicate the corresponding interquartile ranges at each hour.

3.5. Coupling between stomatal conductance and photosynthesis

Heatwaves increased transpiration relative to normal periods for a given CO_2 assimilation rate and VPD (A_n $VPD^{1/2}$) in both chambers (Figure 4a, b; see Sect. 2.7 for methods), indicating weakened coupling between transpiration and photosynthesis. This increase showed up as non-zero water fluxes at zero CO_2 assimilation rate (i.e., the intercept; $p_{int} = 0.009$, Table 1). However, there was no statistically significant difference in the sensitivity of transpiration to A_n $VPD^{1/2}$ (i.e., the slope) between normal periods and heatwaves for the sunlit chamber ($p_{slope} = 0.22$; Figure 4a and Table 1). For the shaded chamber, the difference in the sensitivity of transpiration to A_n $VPD^{1/2}$ was weakly significant ($p_{slope} = 0.027$; Figure 4b and Table 1).

Contrary to the weakened apparent coupling between transpiration and photosynthesis, the composite stomatal sensitivity to the environment, as indicated by the slope parameter (Ball, 1988), did not show statistically significant differences between normal periods and heatwaves in either chamber ($p_{slope} = 0.119$ for sunlit chamber and 0.247 for shaded chamber; Figure 4c, d), nor did the minimum stomatal conductance show any noticeable change (Table 1). Therefore, the composite stomatal sensitivity (m) remained steady and in line with theoretical expectations, even though exceptionally high VPD markedly elevated transpiration (Figure S24, SI) and overwhelmed the effect of partial stomatal closure on transpiration.

Table 1. Test of heatwave effects on the coupling between transpiration and photosynthesis and that between stomatal conductance and photosynthesis. Statistical differences in the intercepts and the slopes between normal periods and heatwaves are tested based on the coefficients of heatwave interaction terms (Sect. 2.7).

	Sunlit chamber			Shaded chamber		
	Coef.	Std. err.	*p*-value	Coef.	Std. err.	*p*-value
Transpiration–photosynthesis coupling						
β_0	0.0244	0.0053	6.0×10^{-6}	0.0132	0.0020	$< 10^{-6}$
β_1	0.0023	0.0001	$< 10^{-6}$	0.0023	0.0001	$< 10^{-6}$
$a_0\beta_0$	0.0440	0.0168	0.009	0.0447	0.0062	$< 10^{-6}$
$a_1\beta_1$	0.0006	0.0005	0.223	0.0004	0.0002	0.027
R^2		0.562			0.805	
Adj. R^2		0.560			0.804	
Stomatal conductance–photosynthesis coupling						
g_0	3.346	0.225	$< 10^{-6}$	3.035	0.224	$< 10^{-6}$
m	2.837	0.137	$< 10^{-6}$	3.524	0.155	$< 10^{-6}$
a_0g_0	–1.110	0.626	0.077	–0.568	0.538	0.292
a_1m	1.996	1.276	0.119	0.870	0.751	0.247
R^2		0.500			0.540	
Adj. R^2		0.497			0.538	

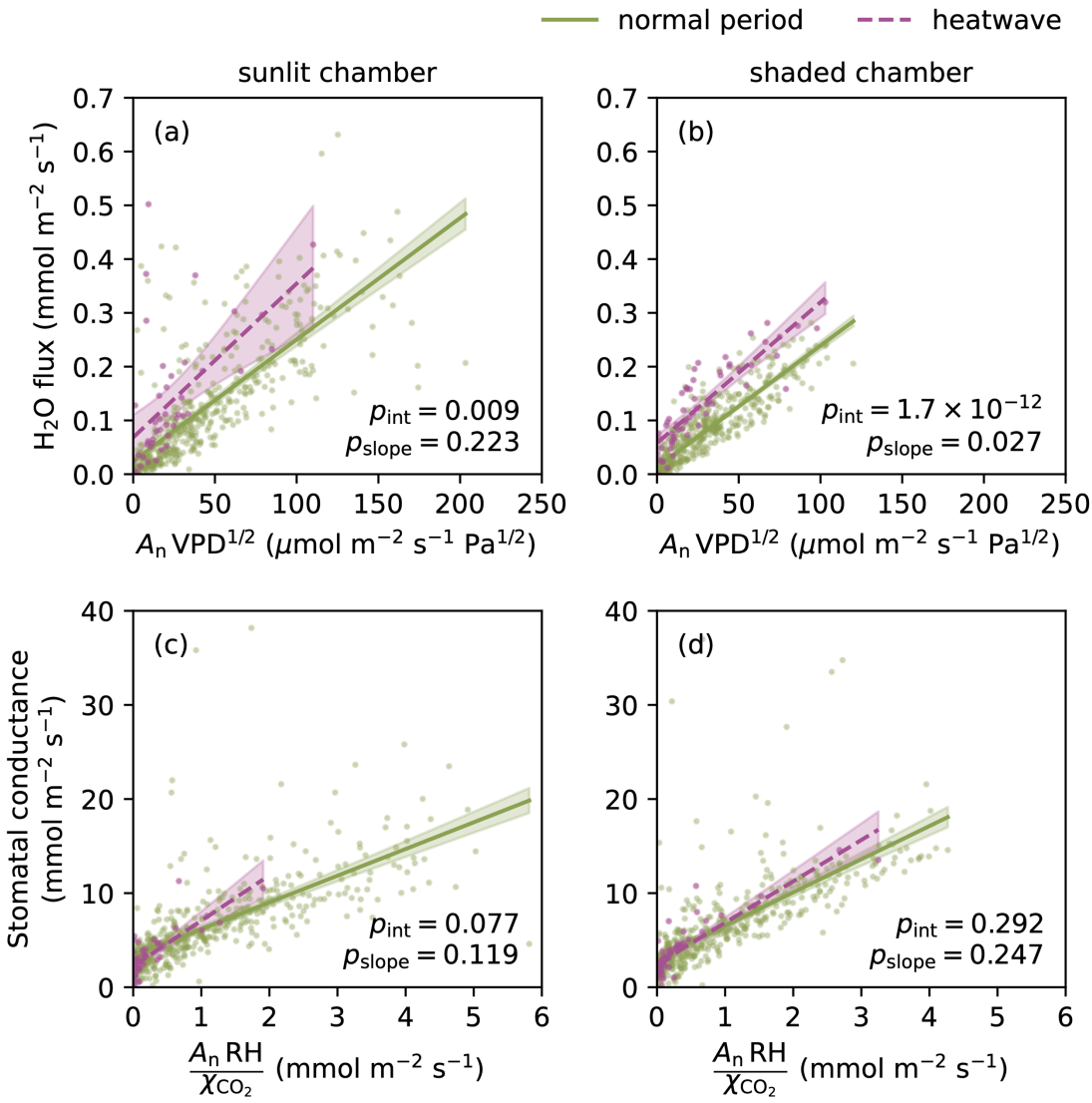

Figure 4. Despite weakening of the coupling between transpiration and photosynthesis, there is little change in the composite stomatal sensitivity to environmental factors between normal periods and heatwaves. (a, b) Distinct relationships of leaf water fluxes as a function of CO_2 assimilation rate and VPD between the normal period (dots and solid lines in olive color) and heatwaves (dots and dashed lines in violet color) in the (a) sunlit and (b) shaded chambers. (c, d) Relationships between stomatal conductance to water vapor and the Ball–Woodrow–Berry predictor for stomatal responses, A_n RH/x_{CO2}, in the (c) sunlit and (d) shaded chambers. Shaded areas around the regression lines indicate 95% confidence intervals. On each panel, the *p*-values characterize the plausibility that the intercepts (p_{int}) or slopes (p_{slope}) are the same between responses in normal periods and heatwaves (null hypothesis) according to a test of the significance of the regression coefficient associated with the heatwave indicator (Sect. 2.7).

3.6. Potential cooling benefits conferred by transpiration–photosynthesis decoupling

Using the fitted relationship between transpiration and photosynthesis for sunlit leaves during normal periods (Figure 4a), we calculated the anticipated transpiration, had the coupling between transpiration and photosynthesis remained the same during heatwaves as normal periods, and inferred the potential cooling benefits resulting from the difference in latent cooling (Figure 5; Sect 2.8). Consistent with the difference in transpiration–photosynthesis coupling (intercept only) between normal periods and heatwaves (Figure 4a), observed transpiration was substantially elevated during heatwaves relative to the counterfactual case of unchanged coupling over most of the day (Figure 5a). However, due to the overall low transpiration rate, the increase in latent heat flux ($\lambda\Delta E$) resulting from the decoupling was moderate, up to 12 W m^{-2} (Figure 5b). This difference translated to a limited leaf cooling effect, up to 0.5°C, when the leaf boundary layer conductance was 0.25 mol m^{-2} s^{-1} (still air conditions; Supplementary Notes S1 and Figure S12, SI), or a negligible cooling effect, up to 0.1°C, when the leaf boundary layer conductance was 2 mol m^{-2} s^{-1} (light breeze conditions; Figure S12, SI). Thus, potential cooling benefits from transpiration–photosynthesis decoupling were likely limited compared with cooling achieved through nonevaporative means.

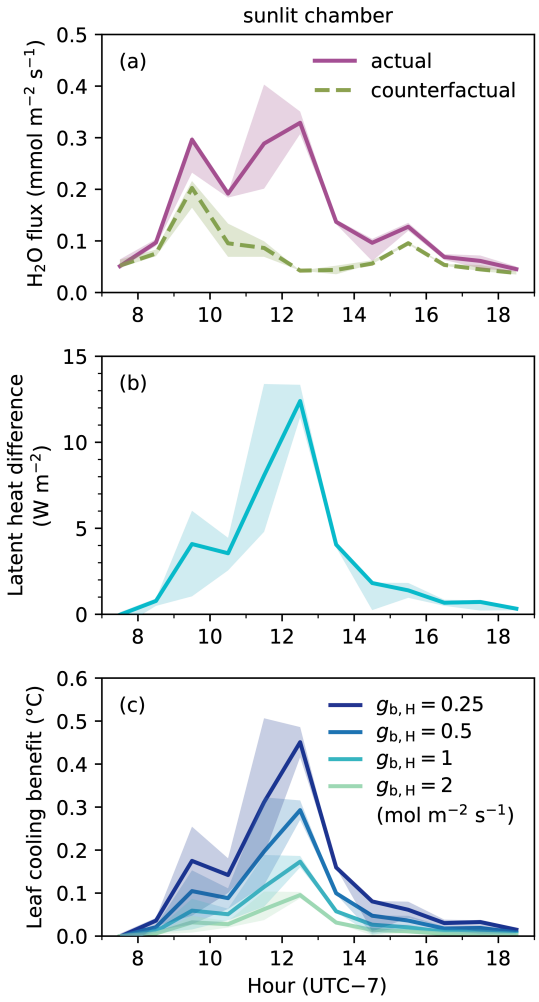

Figure 5. Potential cooling benefits for sunlit leaves conferred by transpiration–photosynthesis decoupling under different turbulent regimes. (a) Observed diurnal cycle of transpiration in the sunlit chamber during heatwaves (solid line in violet color) and the expected diurnal cycle of transpiration had the relationship between transpiration and photosynthesis stayed the same as that during normal periods (i.e., a counterfactual case under the same coupling; dashed line in olive color). (b) Difference in latent heat cooling between the actual (with decoupling) and counterfactual (no decoupling) cases. (c) Diurnal cycles of the latent cooling benefits conferred by transpiration–photosynthesis decoupling under different scenarios of leaf boundary layer conductance to heat, from still air ($g_{b,H}$ = 0.25 mol m^{-2} s^{-1}) to light breeze ($g_{b,H}$ = 2 mol m^{-2} s^{-1}). Lines indicate median diurnal cycles binned by the hour, and shaded areas indicate the corresponding interquartile ranges at each hour.

760 **3.7. Nonstomatal limitation to COS uptake**
761
762 Large and statistically significant differences in stomatal conductance were found between
763 normal periods and heatwaves in both chambers (Figure 6a, b). Here, we focus on stomatal
764 conductance to COS, which is half of stomatal conductance to water vapor due to the lower
765 molecular diffusivity of COS (Eq. 9a; Stimler et al., 2010; Seibt et al., 2010), for comparison with
766 the internal conductance to COS. For the sunlit chamber, stomatal conductance during
767 heatwaves was consistently lower than that in normal periods throughout the day (Figure 6a).
768 For the shaded chamber (Figure 6b), stomatal conductance during heatwaves was lower except
769 in the early morning (06:00–09:00 Pacific Daylight Time) when VPD was not yet high (Figure
770 S24, SI) and photosynthesis was optimal (Figure 3d).
771
772 Internal conductance to COS dropped substantially around noon and in the afternoon (12:00–
773 18:00) during heatwaves in both chambers (Figure 6c, d). No statistically significant differences
774 were found in the morning (06:00–12:00) between normal periods and heatwaves in the sunlit
775 chamber, contrasting the changes in stomatal conductance (Figure 6c vs. a). In the shaded
776 chamber, however, internal conductance to COS showed a statistically significant decrease in the
777 late morning (09:00–12:00). Note that although extreme heat may increase the propensity for
778 leaf COS emissions (Sect. 3.3), given that net COS emissions were still uncommon at
779 temperatures below 40°C (Figure 2; see also Figure S23, SI) and much smaller in magnitude than
780 net COS uptake (compare the 95th and 5th percentile regression lines in Figure 2), the potential
781 leaf COS source is unlikely to impact the median diurnal cycles of the internal conductance to
782 COS.
783
784 The internal diffusion limitation index (Eq. 11 in Sect 2.5), which characterizes the relative
785 importance of internal diffusion limitation vs. stomatal limitation, showed a large but
786 statistically non-significant difference around midday (12:00–15:00) between normal periods
787 and heatwaves for the sunlit chamber (Figure 6e). This lack of statistically significant difference
788 was partly due to the large variability in the internal diffusion limitation index during normal
789 periods (Figure 6e). For the shaded chamber, this index showed a statistically significant increase
790 during heatwaves between mid-morning to early afternoon (09:00–15:00; Figure 6f). Therefore,
791 stomatal limitation and internal diffusion limitation coordinated to suppress photosynthesis
792 during heatwaves, and as indicated by the internal diffusion limitation index, their combined
793 effect peaked around noon.

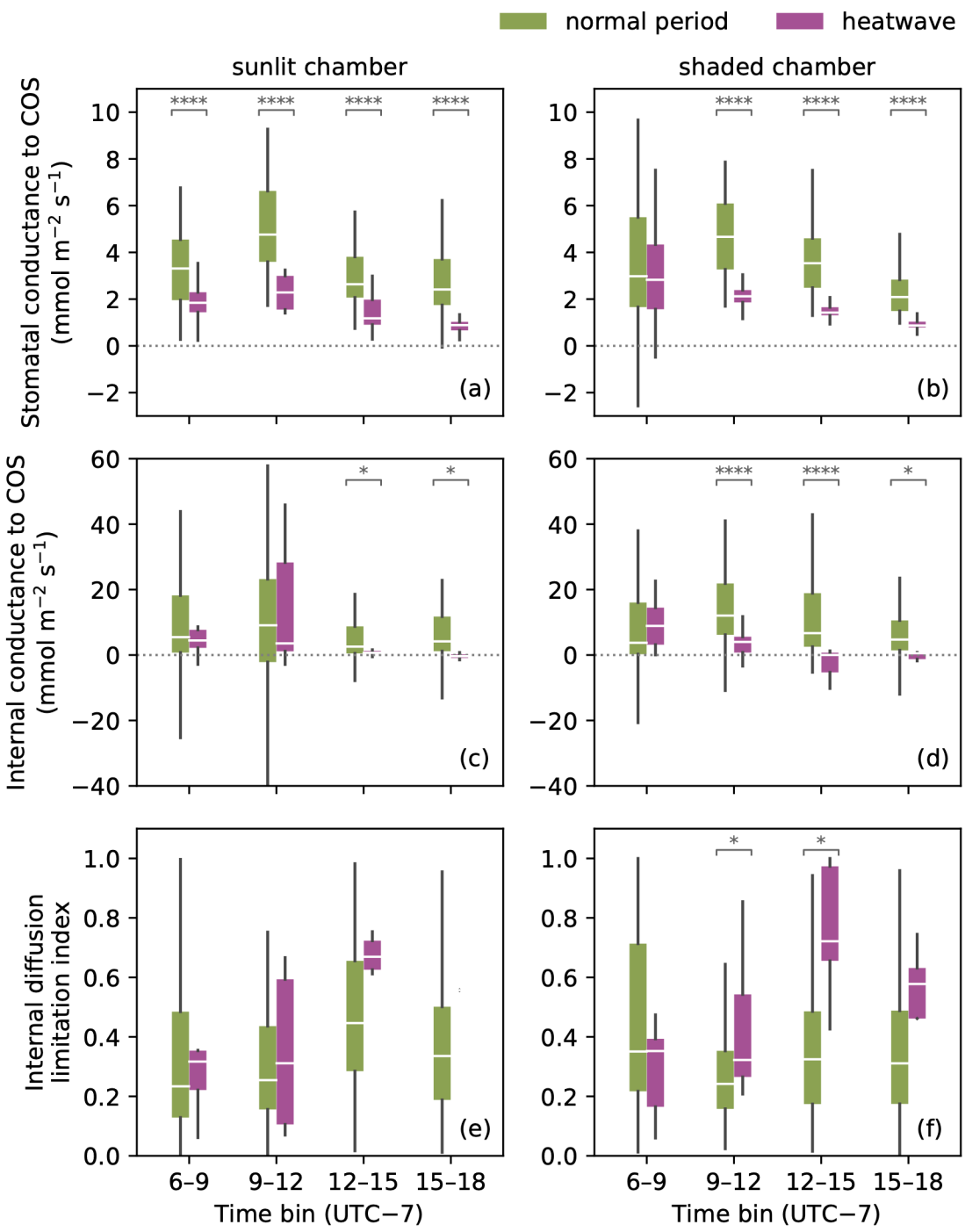

Figure 6. Comparisons of the stomatal conductance to COS (a, b), the internal conductance to COS (c, d), and the internal diffusion limitation index (defined in Eq. 11; e, f) between normal periods (olive color) and heatwaves (violet color) for the sunlit (a, c, e) and shaded (b, d, f) chambers, shown in box plots. Boxes, bars, and whiskers present the interquartile range, medians, and inlier ranges binned by the time of the day in three-hourly bins, respectively. Outliers are omitted for clarity. Stars at the top of each pair of boxes (or lack thereof) indicate

801 the significance level of the difference in the empirical distribution between normal periods and
802 heatwaves according to a two-sample, two-sided Kolmogorov–Smirnov test: '****' – $p < 0.001$;
803 '***' – $p < 0.005$; '**' – $p < 0.01$; '*' – $p < 0.05$; not shown – not significant or test not done due
804 to missing data. Negative estimates of stomatal conductance and internal conductance are
805 preserved in the comparisons to avoid biasing the medians (a–d), but are excluded from the
806 calculation of the internal diffusion limitation index (e, f) to obtain physically meaningful values
807 (Eq. 11 in Sect. 2.5).
808
809 **3.8. Leaf relative uptake between COS and CO_2**
810
811 In both chambers, leaf relative uptake (LRU) between COS and CO_2 showed a typical diurnal
812 response with a minimum around midday (Figure 7a, b), indicating light dependence as the
813 primary control of LRU (Figure S27, SI). This feature of midday LRU minimum was retained
814 during heatwaves, albeit with stronger variability (Figure 7a, b). The midday LRU minima were
815 below 1.0 in both chambers, at the lower end of previously reported light-saturated LRU values
816 across species (0.7–6.2; Stimler et al., 2012; Whelan et al., 2018).
817
818 No statistically significant differences were detected for the LRU in three-hourly diurnal bins
819 between normal periods and heatwaves for the sunlit chamber (Figure 7a). The shaded chamber,
820 by contrast, showed statistically significant differences in LRU between normal periods and
821 heatwaves during mid-morning to early afternoon (09:00–15:00; Figure 7b). For daytime-
822 integrated LRU, neither chamber showed statistically significant differences between normal
823 periods and heatwaves (Figure 7c, d). However, LRU integrated over the whole day differed
824 between the normal periods and heatwaves (Figure 7c). Moreover, as indicated by the
825 interquartile spread (Figure 7c), heatwaves caused stronger day-to-day LRU variability in the
826 sunlit chamber than in the shaded chamber.
827

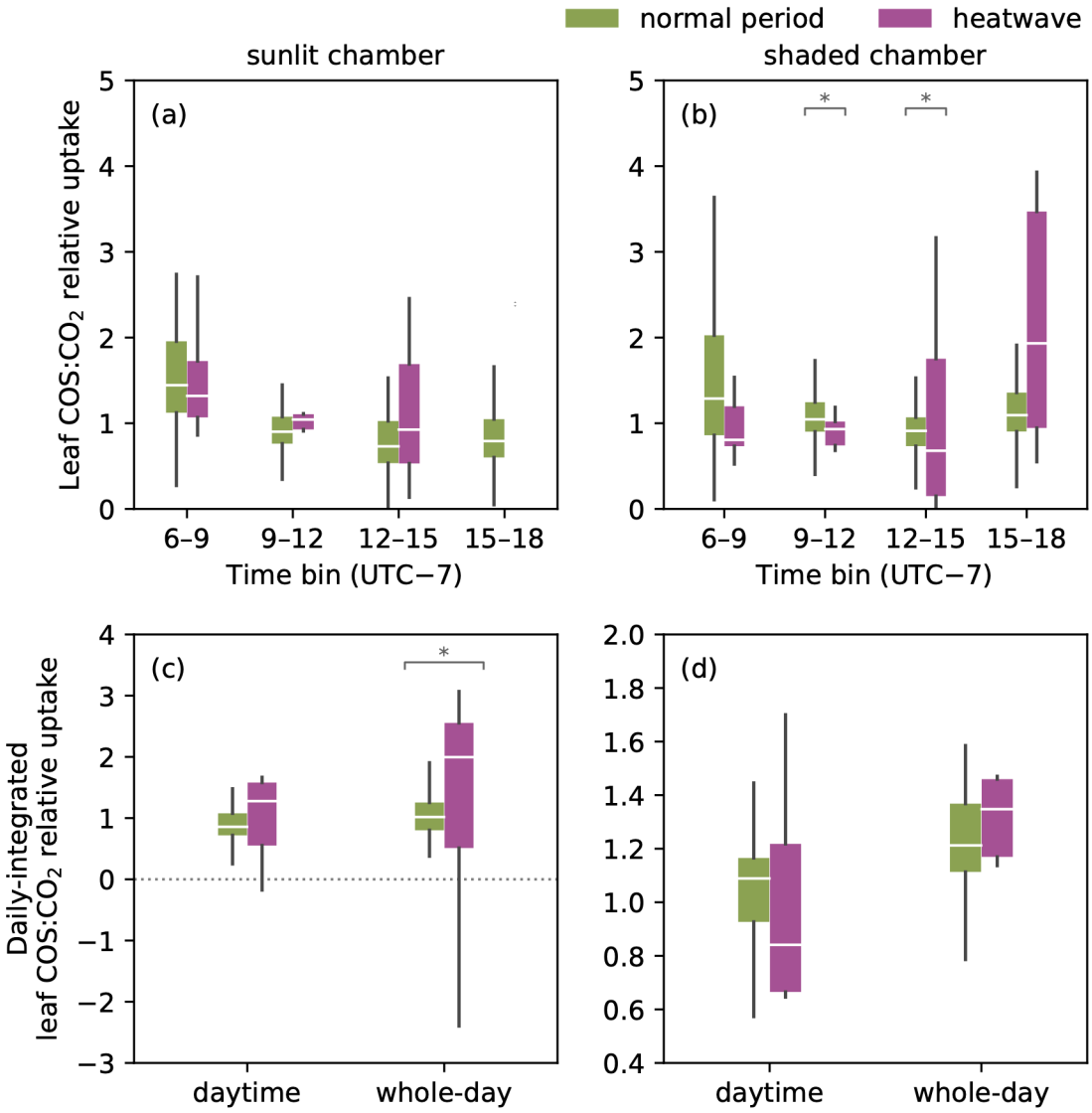

Figure 7. Comparisons of leaf relative uptake between COS and CO_2 (LRU) between normal periods (olive color) and heatwaves (violet color) for the (a, c) sunlit and (b, d) shaded chambers in three-hourly bins (a, b) and at daily integrated timescales (c, d). Note the different scales between (c) and (d). Boxes, bars, and whiskers present the interquartile range, medians, and inlier ranges in each bin (three-hourly, daytime, or whole-day), respectively. Outliers are omitted for clarity. Similar to Figure 6, significance levels are shown for the pair of boxes that have statistically different empirical distributions in a two-sample, two-sided Kolmogorov–Smirnov test. Note that although instantaneous LRU is positive by definition (Eq. 12 in Sect. 2.5), daily-integrated LRU may take negative values due to inclusion of COS emissions during heatwaves (Figure 2).

4. Discussion

4.1. Internal conductance co-limits photosynthesis on the diurnal timescale

Diurnal synchrony between stomatal and internal conductances to COS (Figure 1c, d) indicates that internal diffusion limitation coordinates with stomatal limitation to regulate photosynthesis (Figure 1a, b). This co-limitation also shows up in the midday depression patterns. As the internal conductance to COS dipped below the stomatal conductance to COS around midday (Figure 1c, d), internal diffusion was likely to have become a major limitation on photosynthetic assimilation, contributing to the CO_2 uptake minimum. The internal conductance rebounded after the midday dip (Figure 1c, d), which is in line with the partial afternoon recovery of photosynthesis (Figure 1a, b). These patterns were largely consistent between sunlit and shaded leaves (Figure 1c vs. d) despite their contrasting light and VPD conditions (Figure 1e–h), suggesting that acclimation to canopy microenvironment might have shaped photosynthetic capacity (Figure S16), light responses (Figure S17), intercellular CO_2 concentrations (Figure S18), and diffusional limitations to photosynthesis for optimal canopy-level performance (Campany et al., 2016).

Although the internal conductance to COS incorporates both mesophyll conductance and the catalytic efficiency of carbonic anhydrase in COS hydrolysis (Stimler et al., 2010; Berry et al., 2013; Sun et al., 2022), midday depression in the internal conductance to COS was unlikely to be due to temperature-suppressed carbonic anhydrase activity. Firstly, carbonic anhydrase activity in catalyzing COS hydrolysis is not a major contributor to the variability in the internal conductance to COS (Wehr et al., 2017), possibly due to the high affinity of carbonic anhydrase for COS (Protoschill-Krebs et al., 1996). Secondly, carbonic anhydrase inactivation at maximum daily temperatures within chambers is also unlikely to explain the substantial midday drop in the internal conductance to COS observed here (Figure 1c, d). Though we lack data on the temperature response of carbonic anhydrase activity in *Q. agrifolia*, existing measurements on *Setaria viridis* (C_4) show that carbonic anhydrase activity in catalyzing CO_2 hydration maintains the same level between 30°C and 40°C, the optimum temperature range (Boyd et al., 2015). If this response is representative across species and photosynthetic pathways, it would suggest that even in the sunlit chamber in which maximum daily temperatures routinely reached 40°C (Figure S24a, SI), carbonic anhydrase inactivation was unlikely to limit COS hydrolysis. In the shaded chamber, maximum temperatures on non-heatwave days rarely exceeded 30°C (Figure S24b, SI) and therefore were also not high enough to shut down carbonic anhydrase-mediated COS hydrolysis. Thirdly, the minimal but non-zero net photosynthesis at midday in the sunlit chamber indicates that gross photosynthesis still exceeded mitochondrial respiration and

877 photosynthetic enzyme activities did not shut down completely. Thus, the observed reduction in
878 internal conductance to COS around midday mainly indicates restricted internal diffusion.
879
880 Internal diffusion depends on mesophyll anatomical features and activities of aquaporins and
881 carbon anhydrase in facilitating the aqueous transport (assuming similarity between COS and
882 CO_2 in mesophyll diffusion), with the former responsive to water stress (Clemente-Moreno et
883 al., 2019; Momayyezi et al., 2022) and the latter to both temperature (particularly limitation by
884 low temperatures; Boyd et al., 2015) and water stress (Miyazawa et al., 2008; Guliyev et al.,
885 2008), among other factors. Although water stress increases the intercellular air space and
886 facilitates diffusion therein (Momayyezi et al., 2022), it has also been found to thicken cell walls
887 (Roig-Oliver et al., 2020) and alter cell wall chemical composition (Clemente-Moreno et al.,
888 2019), impeding diffusion across cell walls. Subsequent diffusion across plasma membranes and
889 chloroplast envelopes, presumably mediated by aquaporins (Evans et al., 2009), is enhanced by
890 increasing temperature up to an optimum (von Caemmerer & Evans, 2015; Evans et al., 2021)
891 but restricted by water stress (Miyazawa et al., 2008). As carbonic anhydrase plays an important
892 role in mediating diffusion in the chloroplast stroma (Tholen & Zhu, 2011; Cano et al., 2019;
893 Momayyezi et al., 2020), heat and water stress also affects liquid-phase diffusion through
894 impacts on carbonic anhydrase activity (Boyd et al., 2015; Guliyev et al., 2008). Here, given that
895 VPD and temperature peak at the same time in both chambers (Figure S24, SI), disentangling
896 the impacts of heat and water stress on internal diffusion would require further investigations
897 targeting various structural and metabolic components of mesophyll resistances.
898
899 Moreover, given coordination of mesophyll conductance and photosynthetic activity in
900 sclerophyllous Mediterranean oak species, including *Q. agrifolia* (Peguero-Pina et al., 2017),
901 reduced photosynthetic capacity (electron transport or Rubisco carboxylation) might have also
902 contributed to the observed midday depression in photosynthesis. Limitations from internal
903 diffusion and photosynthetic capacity have both been found to underpin photosynthetic
904 responses to heat and related atmospheric water stress in empirical studies (Sharkey, 2005;
905 Carmo-Silva et al., 2012; Mercado Álvarez et al., 2022; Scafaro et al., 2023) and stomatal
906 optimization theories (e.g., Dewar et al., 2018). It is possible that around midday, the reduction
907 of mesophyll conductance, driven by decreased leaf water potential (Wang et al., 2018; Li et al.,
908 2020) or increased leaf temperature past the optimum (Bernacchi et al., 2002; Evans et al., 2021),
909 and the reduction in photosynthetic capacity (e.g., Mediavilla et al., 2002) join forces to
910 downregulate photosynthesis. Coordinated measurements of leaf gas exchange (COS, CO_2, and
911 water), chlorophyll fluorescence, leaf temperature, and plant water status may help further
912 clarify the roles of mesophyll conductance (including its various anatomical and biochemical

913 determinants) vs. photosynthetic capacity in limiting photosynthesis at the diurnal timescale in
914 dryland ecosystems.
915
916 While mesophyll conductance is routinely measured with leaf-level gas exchange instruments
917 through the variable electron transport (*J*) or isotope discrimination methods, among others
918 (Pons et al., 2009; Cousins et al., 2020), COS as a co-diffusive tracer with CO_2 offers a
919 complementary way to assess internal diffusion limitation, albeit qualitatively for now.
920 Conceptually, COS and water flux measurements used together provide an integral measure of
921 internal diffusion (Eq. 11) without prior information on electron transport, Rubisco parameters,
922 or isotope fractionation factors. This conceptual simplicity, when leveraged along with an
923 autonomous chamber system, has the advantage of enabling continuous monitoring of leaf gas
924 exchange to capture the ofttimes transient impacts of climate extremes on internal diffusion and
925 related physiological parameters. Recent advances in instrumentation (e.g., Magney et al., 2017)
926 that merge leaf gas exchange and optical measurements (e.g., active and passive fluorescence and
927 leaf temperature) appear particularly promising in delivering fine-scale process understanding
928 about the in situ environmental responses of mesophyll conductance. Challenges such as how
929 the mesophyll diffusion pathway of COS differs from that of CO_2 and what roles aquaporins and
930 carbonic anhydrases play in COS aqueous transport remain to be resolved before we can
931 quantitatively interpret the internal conductance to COS and link it to mesophyll conductance
932 to CO_2 derived from well-established methods.
933
934 **4.2. Restricted internal diffusion during heatwaves weakens the coupling between**
935 **transpiration and photosynthesis**
936
937 Heatwaves increased the amount of transpiration needed to sustain the same amount of
938 photosynthesis at the same evaporative demand (Figure 4a, b), leading to weakened leaf-level
939 coupling of transpiration to photosynthesis (Sect. 2.7). Surprisingly, heatwaves did not lead to
940 statistically different responses of stomatal conductance to photosynthesis and environmental
941 variables (Figure 4c, d; Table 1). The steady coupling between stomatal conductance and
942 photosynthesis during heatwaves appears to conflict with the weakened coupling between
943 transpiration and photosynthesis.
944
945 Underlying this ostensible inconsistency in transpiration–photosynthesis coupling is restricted
946 internal diffusion during heatwaves, which suppresses photosynthesis without altering stomatal
947 functions or reducing transpiration to the same extent (Evans et al., 2021). Large and statistically
948 significant reductions in the internal conductance to COS occur around midday and in the
949 afternoon (12:00–18:00 for the sunlit chamber, but 09:00–18:00 for the shaded chamber) during

heatwaves (Figure 6c, d). The reduction in the internal conductance to COS is substantially greater than that in stomatal conductance (Figure 6a, b), indicating a major role of internal diffusion limitation in downregulating photosynthesis while keeping transpiration high relative to normal periods. Given the well-documented role of mesophyll conductance in regulating water use efficiency (Flexas et al., 2013, 2016; Buckley & Warren, 2014; Han et al., 2016; Tomeo & Rosenthal, 2017), it appears that the weakened transpiration–photosynthesis coupling (i.e., abnormally low water use efficiency) does not warrant a revisit to stomatal behavior as described by current empirical or optimality models (Ball, 1988; Leuning, 1995; Medlyn et al., 2011). Rather, environmental responses of mesophyll conductance may need to be explicitly integrated with stomatal conductance models (e.g., Dewar et al., 2018) for predicting transpiration–photosynthesis decoupling.

Contrary to previous whole-tree chamber experiments (e.g., Drake et al., 2018), we found only limited potential cooling benefits (< 0.5°C) granted by heatwave-induced decoupling between transpiration and photosynthesis (Figure 5) following theoretical calculations from an idealized leaf energy balance model (Sect. 2.8). Moreover, the magnitude of potential cooling benefits depends on wind speed (Figure 5c): stronger wind is more effective at equilibrating leaf and air temperatures through sensible heat fluxes (Eq. 17; see also Notes S1, SI), paradoxically negating the additional latent cooling benefits resulting from transpiration–photosynthesis decoupling when air temperature is high (Notes S2 and Figure S13, SI). Thus, in this water-limited Mediterranean ecosystem, transpiration–photosynthesis decoupling seems unlikely to function as a survival strategy to prevent leaf overheating. The limited cooling benefits may have resulted from hydraulic traits and thermal responses of the coast live oak (*Q. agrifolia*) as well as environmental constraints. Firstly, coast live oak has low leaf hydraulic conductance (Pivovaroff et al., 2014) and high resistance to xylem embolism (Skelton et al., 2018) among common woody plant species populating California's Mediterranean-type ecosystems, limiting the rate of transpiration that can be sustained under water stress. Although coast live oak has an intermediate rooting depth (Pivovaroff et al., 2018), this one did not appear to have access to an abundance of root-zone soil moisture given its low rates of photosynthesis and transpiration (e.g., compare to Goulden et al., 1994). Secondly, sclerophyllous oaks, including coast live oak, often have a high critical temperature (up to 56°C) for Photosystem II (Ghouil et al., 2003) and this critical temperature is especially elevated under drought conditions (Ghouil et al., 2003; Gimeno et al., 2009). Hence, it was unlikely for leaves to reach a lethal temperature to necessitate the use of transpiration–photosynthesis decoupling as an emergency measure for heat mitigation. Thirdly, within-canopy turbulence, coupled with adaptive changes in vegetation structure (e.g., leaf shape) to reduce aerodynamic and boundary layer resistances to heat, has been found effective as a non-evaporative means to cooling in a semi-arid forest (Muller et al., 2021). These

987 factors combined suggest that transpiration–photosynthesis decoupling is unlikely to be invoked
988 as a cooling mechanism for coast live oaks in this Mediterranean-climate woodland. More broadly,
989 what plants stand to gain from transpiration–photosynthesis decoupling in a water-limited
990 environment may depend on the species and its hydraulic, photosynthetic, and thermoregulatory
991 traits and must be understood in an integrated framework of water use, carbon metabolism, and
992 thermal regulation.
993
994 In addition to restricted internal diffusion, recent studies show that the weakened transpiration–
995 photosynthesis coupling during heatwaves likely has multiple causes (De Kauwe et al., 2019;
996 Breshears et al., 2021) and may involve canopy structural changes (e.g., Muller et al., 2021) or
997 land–atmosphere feedbacks beyond the scales of leaves and individual trees (Krich et al., 2022).
998 Equally important for the downregulation of photosynthesis under heat stress could be increased
999 photorespiration (Sharkey, 2005), reduced Rubisco enzyme activity as leaf temperature surpasses
1000 the optimum (Carmo-Silva et al., 2012), or increased photoprotective non-photochemical
1001 quenching with temperature (Bilger & Björkman, 1991), none of which seems to directly alter
1002 stomatal sensitivity. Integrating leaf gas exchange measurements—including COS fluxes—in a
1003 leaf energy balance and plant hydraulics framework may help map out the intricate biophysical
1004 and physiological mechanisms underlying transpiration–photosynthesis decoupling at leaf to
1005 ecosystem scales.
1006
1007 **5. Conclusions**
1008
1009 In this Mediterranean-climate oak woodland, midday depression defines the diurnal cycles of leaf
1010 COS and CO_2 fluxes and reflects a shared control on the diffusion of both gases into stomata and
1011 the leaf interior. Internal diffusion limitation plays a significant role in downregulating
1012 photosynthetic assimilation in response to elevated atmospheric water stress, as indicated by the
1013 large diurnal variability in the internal conductance to COS. This finding also shows that
1014 concurrent measurements of leaf COS, CO_2, and water fluxes can help distinguish between
1015 stomatal and nonstomatal limitations to photosynthesis.
1016
1017 Heatwaves that frequent this Mediterranean ecosystem increase both stomatal and internal
1018 diffusion limitations to photosynthesis. This leads to substantial changes to the diurnal cycles of
1019 leaf fluxes. While apparent decoupling between transpiration and photosynthesis has been found
1020 during heatwaves, such decoupling did not result from altered stomatal sensitivity to
1021 environmental factors, but was partly because restricted internal diffusion impacts
1022 photosynthesis and transpiration differently. Leaf energy balance modeling indicates that
1023 increased transpiration resulting from transpiration–photosynthesis decoupling provides limited

cooling benefits, suggesting that decoupling may not act as an effective heat mitigation strategy as previously thought. What triggers the internal diffusion limitation and what physiological function it serves, especially in relation to plant strategies for coping with extreme heat, remain to be clarified through future research.

As arid and semi-arid ecosystems are projected to experience more frequent heat extremes, understanding heatwave impacts on the coupled carbon and water cycles is crucial to assessing the resilience and vulnerability of dryland ecosystems to climate change. In this regard, COS as a multi-scale tracer for carbon and water cycles will help inform an integrative understanding of heatwave impacts across leaf to biome scales. Currently, heatwave impacts on COS fluxes and photosynthesis, particularly at integrated spatial and temporal scales, remain uncertain due to limited field studies targeting dryland ecosystems. Looking forward, more spatially and temporally representative observations of ecosystem COS fluxes and atmospheric COS concentrations will be needed for understanding the responses of transpiration and photosynthesis to heatwaves in global dryland biomes.

Acknowledgements

This work was supported by the European Research Council Starting Grant no. 202835 "COSIRIS" and the NSF CAREER Award no. 1455381 to U.S. W.S. acknowledges support through a graduate student fellowship from the University of California's Institute for the Study of Ecological Effects of Climate Impacts (ISEECI). We thank Philip Rundel and Rasoul Sharifi for support during the field campaign and for helpful discussions, and Joe Berry for valuable feedback on this study. We thank Georg Wohlfahrt, Felix Spielmann, Christopher Still, and an anonymous reviewer for helpful comments. Data supporting this study are made freely available at https://gitlab.com/wusun/stunt-ranch-cos. The authors declare no conflict of interest.

References

Allen, C. D., Breshears, D. D., & McDowell, N. G. (2015). On underestimation of global vulnerability to tree mortality and forest die-off from hotter drought in the Anthropocene. *Ecosphere*, *6*(8), 129. https://doi.org/10.1890/ES15-00203.1

Allen, C. D., Macalady, A. K., Chenchouni, H., Bachelet, D., McDowell, N., Vennetier, M., Kitzberger, T., Rigling, A., Breshears, D. D., Hogg, E. H. (Ted), Gonzalez, P., Fensham, R., Zhang, Z., Castro, J., Demidova, N., Lim, J.-H., Allard, G., Running, S. W., Semerci, A., & Cobb, N. (2010). A global overview of drought and heat-induced tree mortality reveals emerging climate change risks for forests. *Forest Ecology and Management*, *259*(4), 660–684. https://doi.org/10.1016/j.foreco.2009.09.001

Ball, J. T. (1988). *An analysis of stomatal conductance* (pp. 1–89) [PhD thesis]. Stanford University.

Berkelhammer, M., Alsip, B., Matamala, R., Cook, D., Whelan, M. E., Joo, E., Bernacchi, C., Miller, J., & Meyers, T. (2020). Seasonal evolution of canopy stomatal conductance for a prairie and maize field in the Midwestern United States from continuous carbonyl sulfide fluxes. *Geophysical Research Letters*, *47*(6), e2019GL085652. https://doi.org/10.1029/2019GL085652

Bernacchi, C. J., Portis, A. R., Nakano, H., Caemmerer, S. von, & Long, S. P. (2002). Temperature response of mesophyll conductance. Implications for the determination of rubisco enzyme kinetics and for limitations to photosynthesis in vivo. *Plant Physiology*, *130*(4), 1992–1998. https://doi.org/10.1104/pp.008250

Berry, J., Wolf, A., Campbell, J. E., Baker, I., Blake, N., Blake, D., Denning, A. S., Kawa, S. R., Montzka, S. A., Seibt, U., Stimler, K., Yakir, D., & Zhu, Z. (2013). A coupled model of the global cycles of carbonyl sulfide and CO_2: A possible new window on the carbon cycle. *Journal of Geophysical Research: Biogeosciences*, *118*(2), 842–852. https://doi.org/10.1002/jgrg.20068

Bilger, W., & Björkman, O. (1991). Temperature dependence of violaxanthin de-epoxidation and non-photochemical fluorescence quenching in intact leaves of *Gossypium hirsutum* L. and *Malva parviflora* L. *Planta*, *184*(2), 226–234. https://doi.org/10.1007/bf00197951

Blonder, B. W., Aparecido, L. M. T., Hultine, K. R., Lombardozzi, D., Michaletz, S. T., Posch, B. C., Slot, M., & Winter, K. (2023). Plant water use theory should incorporate hypotheses about extreme environments, population ecology, and community ecology. *New Phytologist*. https://doi.org/10.1111/nph.18800

Boyd, R. A., Gandin, A., & Cousins, A. B. (2015). Temperature responses of C_4 photosynthesis: Biochemical analysis of Rubisco, phosphoenolpyruvate carboxylase, and carbonic anhydrase in *Setaria viridis*. *Plant Physiology*, *169*(3), 1850–1861. https://doi.org/10.1104/pp.15.00586

Breshears, D. D., Fontaine, J. B., Ruthrof, K. X., Field, J. P., Feng, X., Burger, J. R., Law, D. J., Kala, J., & Hardy, G. E. St. J. (2021). Underappreciated plant vulnerabilities to heat waves. *New Phytologist*, *231*(1), 32–39. https://doi.org/10.1111/nph.17348

Buckley, T. N. (2017). Modeling stomatal conductance. *Plant Physiology*, *174*(2), 572–582. https://doi.org/10.1104/pp.16.01772

Buckley, T. N., Sack, L., & Farquhar, G. D. (2017). Optimal plant water economy. *Plant, Cell & Environment*, *40*(6), 881–896. https://doi.org/10.1111/pce.12823

Campbell, J. E., Carmichael, G. R., Chai, T., Mena-Carrasco, M., Tang, Y., Blake, D. R., Blake, N. J., Vay, S. A., Collatz, G. J., Baker, I., Berry, J. A., Montzka, S. A., Sweeney, C., Schnoor, J. L., & Stanier, C. O. (2008). Photosynthetic control of atmospheric carbonyl sulfide during the growing season. *Science*, *322*(5904), 1085–1088. https://doi.org/10.1126/science.1164015

Carmo-Silva, A. E., Gore, M. A., Andrade-Sanchez, P., French, A. N., Hunsaker, D. J., & Salvucci, M. E. (2012). Decreased CO_2 availability and inactivation of Rubisco limit photosynthesis in cotton plants under heat and drought stress in the field. *Environmental and Experimental Botany*, *83*, 1–11. https://doi.org/10.1016/j.envexpbot.2012.04.001

Cochavi, A., Amer, M., Stern, R., Tatarinov, F., Migliavacca, M., & Yakir, D. (2021). Differential responses to two heatwave intensities in a Mediterranean citrus orchard are identified by combining measurements of fluorescence and carbonyl sulfide (COS) and CO_2 uptake. *New Phytologist*, *230*(4), 1394–1406. https://doi.org/10.1111/nph.17247

Commane, R., Meredith, L. K., Baker, I. T., Berry, J. A., Munger, J. W., Montzka, S. A., Templer, P. H., Juice, S. M., Zahniser, M. S., & Wofsy, S. C. (2015). Seasonal fluxes of carbonyl sulfide in a midlatitude forest. *Proceedings of the National Academy of Sciences*, *112*(46), 14162–14167. https://doi.org/10.1073/pnas.1504131112

Coumou, D., & Robinson, A. (2013). Historic and future increase in the global land area affected by monthly heat extremes. *Environmental Research Letters*, *8*(3), 034018. https://doi.org/10.1088/1748-9326/8/3/034018

Cowan, I. R. (1977). Stomatal behaviour and environment. *Advances in Botanical Research*, *4*, 117–228. https://doi.org/10.1016/S0065-2296(08)60370-5

Daly, C., Halbleib, M., Smith, J. I., Gibson, W. P., Doggett, M. K., Taylor, G. H., Curtis, J., & Pasteris, P. P. (2008). Physiographically sensitive mapping of climatological temperature and precipitation across the conterminous United States. *International Journal of Climatology*, *28*(15), 2031–2064. https://doi.org/10.1002/joc.1688

De Kauwe, M. G., Medlyn, B. E., Pitman, A. J., Drake, J. E., Ukkola, A., Griebel, A., Pendall, E., Prober, S., & Roderick, M. (2019). Examining the evidence for decoupling between photosynthesis and transpiration during heat extremes. *Biogeosciences*, *16*(4), 903–916. https://doi.org/10.5194/bg-16-903-2019

Dewar, R., Mauranen, A., Mäkelä, A., Hölttä, T., Medlyn, B., & Vesala, T. (2018). New insights into the covariation of stomatal, mesophyll and hydraulic conductances from optimization models incorporating nonstomatal limitations to photosynthesis. *New Phytologist*, *217*(2), 571–585. https://doi.org/10.1111/nph.14848

Drake, J. E., Tjoelker, M. G., Vårhammar, A., Medlyn, B. E., Reich, P. B., Leigh, A., Pfautsch, S., Blackman, C. J., López, R., Aspinwall, M. J., Crous, K. Y., Duursma, R. A., Kumarathunge, D., De Kauwe, M. G., Jiang, M., Nicotra, A. B., Tissue, D. T., Choat, B., Atkin, O. K., & Barton, C. V. M. (2018). Trees tolerate an extreme heatwave via sustained transpirational cooling and increased leaf thermal tolerance. *Global Change Biology*, *24*(6), 2390–2402. https://doi.org/10.1111/gcb.14037

Elliott, S., Lu, E., & Rowland, F. S. (1989). Rates and mechanisms for the hydrolysis of carbonyl sulfide in natural waters. *Environmental Science & Technology*, *23*(4), 458–461. https://doi.org/10.1021/es00181a011

Farquhar, G. D., & Sharkey, T. D. (1982). Stomatal conductance and photosynthesis. *Annual Review of Plant Physiology*, *33*(1), 317–345. https://doi.org/10.1146/annurev.pp.33.060182.001533

Goff, J. A., & Gratch, S. (1946). Low-pressure properties of water from −160 to 212°F. *The 52nd Annual Meeting of the American Society of Heating and Ventilating Engineers*, 95–122.

Griffin, D., & Anchukaitis, K. J. (2014). How unusual is the 2012–2014 California drought? *Geophysical Research Letters*, *41*(24), 9017–9023. https://doi.org/10.1002/2014gl062433

Guliyev, N., Bayramov, S., & Babayev, H. (2008). Effect of water deficit on Rubisco and carbonic anhydrase activities in different wheat genotypes. In J. F. Allen, E. Gantt, J. H. Golbeck, & B. Osmond (Eds.), *Photosynthesis. Energy from the sun* (pp. 1465–1468). Springer Netherlands. https://doi.org/10.1007/978-1-4020-6709-9_315

Horst, S. V. J. van der, Pitman, A. J., De Kauwe, M. G., Ukkola, A., Abramowitz, G., & Isaac, P. (2019). How representative are FLUXNET measurements of surface fluxes during temperature extremes? *Biogeosciences*, *16*(8), 1829–1844. https://doi.org/10.5194/bg-16-1829-2019

Khalifah, R. G. (1971). The carbon dioxide hydration activity of carbonic anhydrase: I. Stop-flow kinetic studies on the native human isoenzymes B and C. *Journal of Biological Chemistry*, *246*(8), 2561–2573. https://doi.org/10.1016/S0021-9258(18)62326-9

Kooijmans, L. M. J., Cho, A., Ma, J., Kaushik, A., Haynes, K. D., Baker, I., Luijkx, I. T., Groenink, M., Peters, W., Miller, J. B., Berry, J. A., Ogée, J., Meredith, L. K., Sun, W., Kohonen, K.-M., Vesala, T., Mammarella, I., Chen, H., Spielmann, F. M., … Krol, M. (2021). Evaluation of carbonyl sulfide biosphere exchange in the Simple Biosphere Model (SiB4). *Biogeosciences*, *18*(24), 6547–6565. https://doi.org/10.5194/bg-18-6547-2021

Kooijmans, L. M. J., Maseyk, K., Seibt, U., Sun, W., Vesala, T., Mammarella, I., Kolari, P., Aalto, J., Franchin, A., Vecchi, R., Valli, G., & Chen, H. (2017). Canopy uptake dominates nighttime carbonyl sulfide fluxes in a boreal forest. *Atmospheric Chemistry and Physics*, *17*(18), 11453–11465. https://doi.org/10.5194/acp-17-11453-2017

Kooijmans, L. M. J., Sun, W., Aalto, J., Erkkilä, K.-M., Maseyk, K., Seibt, U., Vesala, T., Mammarella, I., & Chen, H. (2019). Influences of light and humidity on carbonyl sulfide-based estimates of photosynthesis. *Proceedings of the National Academy of Sciences*, 201807600. https://doi.org/10.1073/pnas.1807600116

Kooijmans, L. M. J., Uitslag, N. A. M., Zahniser, M. S., Nelson, D. D., Montzka, S. A., & Chen, H. (2016). Continuous and high-precision atmospheric concentration measurements of COS, CO_2, CO and H_2O using a quantum cascade laser spectrometer (QCLS). *Atmospheric Measurement Techniques*, *9*(11), 5293–5314. https://doi.org/10.5194/amt-9-5293-2016

Krich, C., Mahecha, M. D., Migliavacca, M., Kauwe, M. G. D., Griebel, A., Runge, J., & Miralles, D. G. (2022). Decoupling between ecosystem photosynthesis and transpiration: A last resort against overheating. *Environmental Research Letters*, *17*(4), 044013. https://doi.org/10.1088/1748-9326/ac583e

Leuning, R. (1995). A critical appraisal of a combined stomatal-photosynthesis model for C_3 plants. *Plant, Cell & Environment*, *18*(4), 339–355. https://doi.org/10.1111/j.1365-3040.1995.tb00370.x

Li, Y., Song, X., Li, S., Salter, W. T., & Barbour, M. M. (2020). The role of leaf water potential in the temperature response of mesophyll conductance. *New Phytologist*, *225*(3), 1193–1205. https://doi.org/10.1111/nph.16214

Maignan, F., Abadie, C., Remaud, M., Kooijmans, L. M. J., Kohonen, K.-M., Commane, R., Wehr, R., Campbell, J. E., Belviso, S., Montzka, S. A., Raoult, N., Seibt, U., Shiga, Y. P., Vuichard, N., Whelan, M. E., & Peylin, P. (2021). Carbonyl sulfide: Comparing a mechanistic representation of the vegetation uptake in a land surface model and the leaf relative uptake approach. *Biogeosciences*, *18*(9), 2917–2955. https://doi.org/10.5194/bg-18-2917-2021

Mediavilla, S., Santiago, H., & Escudero, A. (2002). Stomatal and mesophyll limitations to photosynthesis in one evergreen and one deciduous Mediterranean oak species. *Photosynthetica*, *40*(4), 553–559. https://doi.org/10.1023/a:1024399919107

Medlyn, B. E., Duursma, R. A., Eamus, D., Ellsworth, D. S., Prentice, I. C., Barton, C. V. M., Crous, K. Y., De Angelis, P., Freeman, M., & Wingate, L. (2011). Reconciling the optimal and empirical approaches to modelling stomatal conductance. *Global Change Biology*, *17*(6), 2134–2144. https://doi.org/10.1111/j.1365-2486.2010.02375.x

Mercado Álvarez, K., Bertero, H. D., Paytas, M. J., & Ploschuk, E. L. (2022). Mesophyll conductance modulates photosynthetic rate in cotton crops exposed to heat stress under

field conditions. *Journal of Agronomy and Crop Science*, *208*(1), 53–64. https://doi.org/10.1111/jac.12536

Momayyezi, M., Borsuk, A. M., Brodersen, C. R., Gilbert, M. E., Théroux-Rancourt, G., Kluepfel, D. A., & McElrone, A. J. (2022). Desiccation of the leaf mesophyll and its implications for CO_2 diffusion and light processing. *Plant, Cell & Environment*, *45*(5), 1362–1381. https://doi.org/10.1111/pce.14287

Montzka, S. A., Calvert, P., Hall, B. D., Elkins, J. W., Conway, T. J., Tans, P. P., & Sweeney, C. (2007). On the global distribution, seasonality, and budget of atmospheric carbonyl sulfide (COS) and some similarities to CO_2. *Journal of Geophysical Research: Atmospheres*, *112*(D9), D09302. https://doi.org/10.1029/2006JD007665

Mu, M., De Kauwe, M. G., Ukkola, A. M., Pitman, A. J., Guo, W., Hobeichi, S., & Briggs, P. R. (2021). Exploring how groundwater buffers the influence of heatwaves on vegetation function during multi-year droughts. *Earth System Dynamics*, *12*(3), 919–938. https://doi.org/10.5194/esd-12-919-2021

Myneni, R. B. (2020). *MODIS Collection 6 (C6) LAI/FPAR product user's guide* (p. 13). https://lpdaac.usgs.gov/documents/624/MOD15_User_Guide_V6.pdf

Myneni, R. B., Hoffman, S., Knyazikhin, Y., Privette, J. L., Glassy, J., Tian, Y., Wang, Y., Song, X., Zhang, Y., Smith, G. R., Lotsch, A., Friedl, M., Morisette, J. T., Votava, P., Nemani, R. R., & Running, S. W. (2002). Global products of vegetation leaf area and fraction absorbed PAR from year one of MODIS data. *Remote Sensing of Environment*, *83*(1-2), 214–231. https://doi.org/10.1016/s0034-4257(02)00074-3

Nelson, D. (2012). *TDLWintel User's Manual* (pp. 1–87). Aerodyne Research, Inc., Billerica, MA, USA.

Nelson, J. A., Pérez-Priego, O., Zhou, S., Poyatos, R., Zhang, Y., Blanken, P. D., Gimeno, T. E., Wohlfahrt, G., Desai, A. R., Gioli, B., Limousin, J.-M., Bonal, D., Paul-Limoges, E., Scott, R. L., Varlagin, A., Fuchs, K., Montagnani, L., Wolf, S., Delpierre, N., … Jung, M. (2020). Ecosystem transpiration and evaporation: Insights from three water flux partitioning methods across FLUXNET sites. *Global Change Biology*, *26*(12), 6916–6930. https://doi.org/https://doi.org/10.1111/gcb.15314

Ögren, E., & Evans, J. R. (1993). Photosynthetic light-response curves: I. The influence of CO_2 partial pressure and leaf inversion. *Planta*, *189*(2), 182–190. https://doi.org/10.1007/bf00195075

Peguero-Pina, J. J., Sisó, S., Flexas, J., Galmés, J., García-Nogales, A., Niinemets, Ü., Sancho-Knapik, D., Saz, M. Á., & Gil-Pelegrín, E. (2017). Cell-level anatomical characteristics explain high mesophyll conductance and photosynthetic capacity in sclerophyllous Mediterranean oaks. *New Phytologist*, *214*(2), 585–596. https://doi.org/10.1111/nph.14406

Pivovaroff, A. L., Cook, V. M. W., & Santiago, L. S. (2018). Stomatal behaviour and stem xylem traits are coordinated for woody plant species under exceptional drought conditions. *Plant, Cell & Environment*, *41*(11), 2617–2626. https://doi.org/10.1111/pce.13367

PRISM Climate Group, Oregon State University. (2021). *PRISM Spatial Climate Datasets for the Conterminous United States*. http://prism.oregonstate.edu/.

Protoschill-Krebs, G., Wilhelm, C., & Kesselmeier, J. (1996). Consumption of carbonyl sulphide (COS) by higher plant carbonic anhydrase (CA). *Atmospheric Environment*, *30*(18), 3151–3156. https://doi.org/10.1016/1352-2310(96)00026-X

Rastogi, B., Berkelhammer, M., Wharton, S., Whelan, M. E., Itter, M. S., Leen, J. B., Gupta, M. X., Noone, D., & Still, C. J. (2018b). Large uptake of atmospheric OCS observed at a moist old growth forest: Controls and implications for carbon cycle applications. *Journal of Geophysical Research: Biogeosciences*, *123*(11), 3424–3438. https://doi.org/10.1029/2018JG004430

Schenk, S., Kesselmeier, J., & Anders, E. (2004). How does the exchange of one oxygen atom with sulfur affect the catalytic cycle of carbonic anhydrase? *Chemistry – A European Journal*, *10*(12), 3091–3105. https://doi.org/10.1002/chem.200305754

Seibt, U., Kesselmeier, J., Sandoval-Soto, L., Kuhn, U., & Berry, J. A. (2010). A kinetic analysis of leaf uptake of COS and its relation to transpiration, photosynthesis and carbon isotope fractionation. *Biogeosciences*, *7*(1), 333–341. https://doi.org/10.5194/bg-7-333-2010

Sentis, A., Hemptinne, J.-L., & Brodeur, J. (2013). Effects of simulated heat waves on an experimental plant–herbivore–predator food chain. *Global Change Biology*, *19*(3), 833–842. https://doi.org/10.1111/gcb.12094

Sharkey, T. D. (2005). Effects of moderate heat stress on photosynthesis: Importance of thylakoid reactions, rubisco deactivation, reactive oxygen species, and thermotolerance provided by isoprene. *Plant, Cell & Environment*, *28*(3), 269–277. https://doi.org/10.1111/j.1365-3040.2005.01324.x

Skelton, R. P., Dawson, T. E., Thompson, S. E., Shen, Y., Weitz, A. P., & Ackerly, D. (2018). Low vulnerability to xylem embolism in leaves and stems of North American oaks. *Plant Physiology*, *177*(3), 1066–1077. https://doi.org/10.1104/pp.18.00103

Sperry, J. S., Venturas, M. D., Anderegg, W. R. L., Mencuccini, M., Mackay, D. S., Wang, Y., & Love, D. M. (2017). Predicting stomatal responses to the environment from the optimization of photosynthetic gain and hydraulic cost. *Plant, Cell & Environment*, *40*(6), 816–830. https://doi.org/10.1111/pce.12852

Spielmann, F. M., Wohlfahrt, G., Hammerle, A., Kitz, F., Migliavacca, M., Alberti, G., Ibrom, A., El-Madany, T. S., Gerdel, K., Moreno, G., Kolle, O., Karl, T., Peressotti, A., & Delle Vedove, G. (2019). Gross primary productivity of four European ecosystems constrained by joint

CO_2 and COS flux measurements. *Geophysical Research Letters*, *46*(10), 5284–5293. https://doi.org/10.1029/2019gl082006

Stimler, K., Berry, J. A., Montzka, S. A., & Yakir, D. (2011). Association between carbonyl sulfide uptake and $^{18}\Delta$ during gas exchange in C_3 and C_4 leaves. *Plant Physiology*, *157*(1), 509–517. https://doi.org/10.1104/pp.111.176578

Stimler, K., Berry, J. A., & Yakir, D. (2012). Effects of carbonyl sulfide and carbonic anhydrase on stomatal conductance. *Plant Physiology*, *158*(1), 524–530. https://doi.org/10.1104/pp.111.185926

Stimler, K., Montzka, S. A., Berry, J. A., Rudich, Y., & Yakir, D. (2010). Relationships between carbonyl sulfide (COS) and CO_2 during leaf gas exchange. *New Phytologist*, *186*(4), 869–878. https://doi.org/10.1111/j.1469-8137.2010.03218.x

Stoy, P. C., El-Madany, T. S., Fisher, J. B., Gentine, P., Gerken, T., Good, S. P., Klosterhalfen, A., Liu, S., Miralles, D. G., Perez-Priego, O., Rigden, A. J., Skaggs, T. H., Wohlfahrt, G., Anderson, R. G., Coenders-Gerrits, A. M. J., Jung, M., Maes, W. H., Mammarella, I., Mauder, M., … Wolf, S. (2019). Reviews and syntheses: Turning the challenges of partitioning ecosystem evaporation and transpiration into opportunities. *Biogeosciences*, *16*(19), 3747–3775. https://doi.org/10.5194/bg-16-3747-2019

Sun, F., Walton, D. B., & Hall, A. (2015). A hybrid dynamical–statistical downscaling technique. Part II: End-of-century warming projections predict a new climate state in the Los Angeles region. *Journal of Climate*, *28*(12), 4618–4636. https://doi.org/10.1175/JCLI-D-14-00197.1

Sun, W. (2018). *PyChamberFlux: A package for calculating trace gas fluxes from chamber measurements (version 0.1.13.a)*. https://doi.org/10.5281/zenodo.1197330

Sun, W., Berry, J. A., Yakir, D., & Seibt, U. (2022). Leaf carbonyl sulfide to CO_2 relative uptake seen through the lens of stomatal conductance–photosynthesis coupling. *New Phytologist*, *235*(5), 1729–1742. https://doi.org/10.1111/nph.18178

Sun, W., Maseyk, K., Lett, C., & Seibt, U. (2016). Litter dominates surface fluxes of carbonyl sulfide in a Californian oak woodland. *Journal of Geophysical Research: Biogeosciences*, *121*(2), 438–450. https://doi.org/10.1002/2015jg003149

Sun, W., Maseyk, K., Lett, C., & Seibt, U. (2018). Stomatal control of leaf fluxes of carbonyl sulfide and CO_2 in a *Typha* freshwater marsh. *Biogeosciences*, *15*(11), 3277–3291. https://doi.org/10.5194/bg-15-3277-2018

Tatarinov, F., Rotenberg, E., Maseyk, K., Ogée, J., Klein, T., & Yakir, D. (2016). Resilience to seasonal heat wave episodes in a Mediterranean pine forest. *New Phytologist*, *210*(2), 485–496. https://doi.org/10.1111/nph.13791

Urban, J., Ingwers, M. W., McGuire, M. A., & Teskey, R. O. (2017). Increase in leaf temperature opens stomata and decouples net photosynthesis from stomatal conductance in *Pinus*

taeda and *Populus deltoides x nigra*. *Journal of Experimental Botany*, *68*(7), 1757–1767. https://doi.org/10.1093/jxb/erx052

Virtanen, P., Gommers, R., Oliphant, T. E., Haberland, M., Reddy, T., Cournapeau, D., Burovski, E., Peterson, P., Weckesser, W., Bright, J., Walt, S. J. van der, Brett, M., Wilson, J., Millman, K. J., Mayorov, N., Nelson, A. R. J., Jones, E., Kern, R., Larson, E., … SciPy 1.0 Contributors. (2020). SciPy 1.0: Fundamental algorithms for scientific computing in Python. *Nature Methods*, *17*(3), 261–272. https://doi.org/10.1038/s41592-019-0686-2

Wang, X., Du, T., Huang, J., Peng, S., & Xiong, D. (2018). Leaf hydraulic vulnerability triggers the decline in stomatal and mesophyll conductance during drought in rice. *Journal of Experimental Botany*, *69*(16), 4033–4045. https://doi.org/10.1093/jxb/ery188

Wehr, R., Commane, R., Munger, J. W., McManus, J. B., Nelson, D. D., Zahniser, M. S., Saleska, S. R., & Wofsy, S. C. (2017). Dynamics of canopy stomatal conductance, transpiration, and evaporation in a temperate deciduous forest, validated by carbonyl sulfide uptake. *Biogeosciences*, *14*(2), 389–401. https://doi.org/10.5194/bg-14-389-2017

Whelan, M. E., Lennartz, S. T., Gimeno, T. E., Wehr, R., Wohlfahrt, G., Wang, Y., Kooijmans, L. M. J., Hilton, T. W., Belviso, S., Peylin, P., Commane, R., Sun, W., Chen, H., Kuai, L., Mammarella, I., Maseyk, K., Berkelhammer, M., Li, K.-F., Yakir, D., … Campbell, J. E. (2018). Reviews and syntheses: Carbonyl sulfide as a multi-scale tracer for carbon and water cycles. *Biogeosciences*, *15*(12), 3625–3657. https://doi.org/10.5194/bg-15-3625-2018

Wohlfahrt, G., Brilli, F., Hörtnagl, L., Xu, X., Bingemer, H., Hansel, A., & Loreto, F. (2012). Carbonyl sulfide (COS) as a tracer for canopy photosynthesis, transpiration and stomatal conductance: Potential and limitations. *Plant, Cell & Environment*, *35*(4), 657–667. https://doi.org/10.1111/j.1365-3040.2011.02451.x

Zhou, S., Yu, B., Huang, Y., & Wang, G. (2014). The effect of vapor pressure deficit on water use efficiency at the subdaily time scale. *Geophysical Research Letters*, *41*(14), 5005–5013. https://doi.org/10.1002/2014GL060741

Zhou, S., Yu, B., Zhang, Y., Huang, Y., & Wang, G. (2016). Partitioning evapotranspiration based on the concept of underlying water use efficiency. *Water Resources Research*, *52*(2), 1160–1175. https://doi.org/10.1002/2015WR017766